Late Holocene great earthquakes in the eastern part of the Aleutian megathrust

Ian Shennan[1], Ronald Bruhn[2], Natasha Barlow[1], Kelly Good[2], Emma Hocking[1,3]

[1] *Sea Level Research Unit, Department of Geography, Durham University, Durham, DH1 3LE, UK*

[2]*Department of Geology and Geophysics, University of Utah, Salt Lake City, UT 84112-0111, USA*

[3] *Current address: Department of Geography, Northumbria University, Newcastle upon Tyne, NE1 8ST, UK*

ABSTRACT

The great earthquake, M_w 9.2, of AD 1964 may not be typical of other megathrust earthquakes in the region during the last 4000 years. We present new field data from three sites: Copper River Delta, the lower Katalla River valley and Puffy Slough, to enhance the temporal and spatial resolutions of the paleoseismic records of multiple great earthquakes. Differences in the spatial patterns of coseismic uplift and subsidence suggest different rupture combinations of the Kodiak, Prince William Sound and western Yakutat segments of the plate boundary. The longest and most comprehensive records all come from the Prince William Sound segment. Most sites here reveal net subsidence over multiple earthquake cycles except where probable upper plate faulting contributes locally to net uplift, with measurable differences between sites only a few kilometers apart. We identify the Katalla area as a source of local seismic hazard, similar to other locations in the western part of the Yakutat microplate, including the two Mw8+ ruptures in AD 1899. We use a Bayesian radiocarbon modeling

approach to estimate the age and recurrence intervals of multiple great earthquakes for the Prince William Sound segment of the megathrust. The long interval, 883 ± 34 (2σ) years, between the penultimate earthquake and AD 1964 contrasts with the older earthquakes that have intervals ranging from ~420 to ~610 years, with a mean of ~535 years.

1. INTRODUCTION

Paleoseismological investigations provide both major inputs and challenges for seismic hazard assessment. While the classic notion of the characteristic earthquake, with constant dimensions and recurrence interval over multiple earthquake cycles, forms the basis for the time-independent seismic hazard maps of Alaska (Wesson et al., 2007), the growth of paleoseismological studies and improvements in analytical methods (Boyd et al., 2008) raise fundamental questions that require further analysis, including segmentation and magnitude-frequency relationships (Wesson et al., 2008). The great Alaskan earthquake, M_w9.2, of March 1964, ruptured ~950 km of the Aleutian megathrust, encompassing the Kodiak and Prince William Sound segments (Carver and Plafker, 2008), and resulted in coseismic uplift adjacent to the trench and a zone of subsidence to the north and northwest (Figure 1).

Coastal marshes can register coseismic vertical land motions through changes in sediment lithology and biostratigraphy, providing records of 1964 and previous great earthquakes. The latest of these occurred ~500 years ago and ruptured only the Kodiak

segment (Carver and Plafker, 2008), while correlation of radiocarbon ages suggest earlier great earthquakes involved either multi-segment ruptures or closely timed sequences of single segment ruptures (Carver and Plafker, 2008; Hutchinson and Crowell, 2007; Shennan et al., 2009). The longest records come from the eastern part of the Prince William Sound segment, at Copper River Delta, with ten great earthquakes since ~5000 cal yr BP (Carver and Plafker, 2008). Farther east, uplifted coastal sediments suggest that earthquakes ~900 and ~1500 years ago may have simultaneously ruptured adjacent segments of the Aleutian megathrust and the Yakutat microplate (Shennan et al., 2009).

Here we use new field data from Copper River Delta, the lower Katalla river valley and Puffy Slough (Figure 2) to enhance the temporal and spatial resolutions of the paleoseismic records of multiple great earthquakes. We provide a new synthesis and temporal model of earthquake recurrence through the Late Holocene using the Bayesian modeling approach outlined by Lienkaemper and Bronk Ramsey (2009) and aim to explain variations in the spatial pattern of coseismic deformation between sites during the Late Holocene.

2. FIELD AND LABORATORY METHODS

In analyzing coastal sediment sequences, four critical criteria help determine a co-seismic signal and discriminate from non-seismic processes that might cause abrupt wetland submergence or emergence: lateral extent of peat-mud couplets with sharp contacts; suddenness of subsidence or emergence; amount of vertical motion; and

synchroneity with other sites (Nelson et al., 1996). Presence of tsunami sediments may also help in certain geographical settings. We use exposures and sediment cores to assess the lithological evidence for these criteria, diatom-based transfer function models to quantify the vertical motion, and AMS radiocarbon dating of *in situ* herbaceous macrofossils to provide a chronology for each site. For the transfer function models we use a regional-scale modern training set collected from a wide range of marshes across ~1000 km of south central Alaska in order to seek the best fit between fossil and modern diatom assemblages (Watcham et al., 2013). We use three models, constrained by the lithology of the Holocene sediment sequence (Table 1); one for peat sediment, a second for silt units with visible plant rootlets and a third for silt units with no rootlets (Hamilton and Shennan, 2005). We assess goodness of fit between each fossil sample and the modern dataset using a dissimilarity coefficient, using the 20th percentile of the dissimilarity values for the modern samples as the cut-off between 'close' and 'poor' modern analogues for fossil samples, and the 5th percentile as the threshold for defining 'good' modern analogues (Hamilton and Shennan, 2005). For reconstructions of the elevation at which the fossil sediment was laid down, termed paleo marsh surface elevation, we present sample-specific 95% error terms.

3. NEW FIELD DATA

3.1 Copper River Delta

During the 1964 earthquake the delta was raised on the order of 2 to 3 m (McCalpin and Carver, 2009; Plafker, 1969). Previous investigations record up to nine pre-1964

93 earthquakes, revealed by multiple couplets of silt overlain by peat, representing
94 coseismic uplift of intertidal mud flats, colonization by freshwater marshes, and gradual
95 interseismic subsidence (Carver and Plafker, 2008; Plafker et al., 1992). The vertical
96 sequence of couplets seen in cores, some more than 11 m in depth, and sections
97 indicates net submergence over multiple earthquake cycles, i.e. the sum of non-seismic
98 relative sea-level change (glacio-isostasy and eustasy), sediment compaction and inter-
99 seismic subsidence is greater than coseismic uplift.
100
101 Two pre-1964 silt-peat sequences are widely exposed in the uppermost ~4 m of the
102 delta sediments exposed along tidal channels (Figure 3) but correlation of some of the
103 older couplets recorded from coring is problematical (Carver and Plafker, 2008). Our
104 primary aim of collecting new material from Copper River Delta was to obtain estimates
105 of the coseismic uplift for different Late Holocene earthquakes. We sampled at three
106 locations along an 8 km stretch of Alaganik Slough (Figure 4), one of the tributaries in
107 the delta west of the main river, using exposures and cores to establish the lateral
108 continuity of each silt-peat couplet in the field.
109
110 Our diatom analyses highlight a key challenge of reconstructing land-level changes in
111 this large delta. We found highly variable diatom preservation in the silt units. For each
112 silt-peat couplet sampled and dated (Table 2) we could count sufficient diatoms in the
113 silt unit to at least confirm formation within an intertidal environment but about half of the
114 samples had insufficient numbers to reach the minimum sum, 200, that we consider
115 suitable for quantitative analysis. We believe one of the major controls on diatom

abundance in tidal silt is the very high sediment concentration of the Copper River, the delta and adjacent coastal waters. Of the surface samples we collected from Copper River Delta to contribute to the modern training set described above, 14 of the 26 that came from unvegetated tidal flat contained insufficient diatom numbers to reach the minimum count so it is perhaps not unexpected to encounter similar limitations with fossil sequences.

The most complete records are for the youngest pre-1964 silt-peat couplet, sampled at all three sites. Diatom assemblages (Figure 4) record the greatest changes in salinity at the most seaward site, 3, with lesser changes progressively upstream, as expected where the influence of freshwater discharge becomes more dominant. At site 3 the transfer function model estimates coseismic uplift ~1.3 m (Figure 5), at site 2 it is in the order of 0.5 m, but with overlapping error terms, and at site 1 there is no clear change in elevation. This may reflect the true pattern of differential uplift but it may also reflect the increasing importance of river discharge as the controlling variable in sedimentation with increasing distance from the open coast. For example, had we only studied this couplet in the area around site 1 we would not be able to satisfy the demonstrable vertical motion criterion outlined by Nelson et al. (1996) for attributing a couplet to a great earthquake. In large coastal systems we recognize that certain areas will be sensitive recorders of rapid emergence or submergence whereas other parts of the system are relatively insensitive, as other parameters become more important controls on sedimentation.

The radiocarbon age for the peat-silt couplet at site 1 also illustrate the limitations of dating just the base of the peat unit as there may be a hiatus following uplift before plant colonization and peat accumulation. It is preferable to bracket the event horizon with two or more dated samples (Carver and Plafker, 2008; Shennan et al., 2009).

Low diatom abundances prevent us obtaining quantitative reconstructions for the older couplets, except for the middle peat at site 3, where estimated uplift is ~1.1 m. We note that the samples from this peat have poor modern analogues but their reconstructed elevations are very similar to all the other samples from peat layers (Figure 5). In a following section we consider this issue further alongside others that may complicate the reconstruction of coseismic uplift.

3.2 Katalla River Valley

The Ragged Mountain Fault is located along the west side of the Katalla valley and marks the western edge of the Yakutat Microplate (Figure 1). At the mouth of the Katalla River, coseismic uplift of 1 to 3 m in 1964 raised the tidal marshes in the lee of a vegetated storm ridge above the elevation of storm tides (McCalpin and Carver, 2009; Plafker, 1969). Numerous prominent ridges occur upstream with low lying marshes between them (Figure 6). Strata within the marshes record a Late Holocene archive of net coastal progradation and relative land and sea-level change driven by repeated cycles of coseismic uplift, interseismic relative sea-level rise/land subsidence, glacio-isostasy and eustasy (McCalpin and Carver, 2009; Plafker, 1969; Richards, 2000; Sirkin and Tuthill, 1971). A silt horizon, at river level and ~7 m above mean sea level

(Richards, 2000; Sirkin and Tuthill, 1971) contains mollusc species indicative of intertidal conditions and dated to ~7 ka BP. Assuming a tidal range similar to present (MHHW ~+1.55 m MSL and HAT ~2.65 m MSL), the mollusc bed indicates at least 4.35 m relative uplift over the past 7000 years. Sirkin and Tuthill (1971) indicate even older marine deposits, >14 ka BP, may occur further up the valley.

The marsh stratigraphy between the ridges in the lower valley (Figure 6) provides evidence of five episodes of coseismic uplift prior to 1964. The oldest is a minimum limiting age of ~2650 – 2350 cal yr BP obtained from the base of peat overlying silt, in marsh 5, location 5.3 (Figure 6). None of the samples contained sufficient diatom abundances to provide quantitative reconstructions but the species present across this abrupt silt-peat couplet, which could be traced laterally in a series of cores, indicate freshwater marsh developed on uplifted intertidal sediment. The gradual transition up the core from peat to silt indicates relative sea-level rise and return to intertidal sedimentation. The same location records a second cycle of coseismic uplift, minimum limiting age, ~2120 – 1950 cal yr BP, and interseismic relative sea-level rise.

We infer the next uplift event from the incision of intertidal/subtidal sand that is abruptly overlain by lagoon mud at location 3.1, dated ~1510 – 1340 cal yr BP. Plant macrofossils within the top of the silt unit and the base of the surface peat of marshes 3, 4 and 5 bracket the next earthquake horizon between 1120 – 960 cal yr BP and the three minimum ages 930 – 790, 790 – 690 and 760 – 680 cal yr BP (Figure 6). Diatom abundances were low in most samples across each of these silt-peat contacts; only that

from location 3.1 containing sufficient numbers to allow quantitative reconstructions of elevation. Frequencies of individual species and the salinity summary classes show a distinct change across the contact (Figure 7), with possibly some mixing within the top 2 cm of the silt horizon. Transfer function reconstructions indicate uplift in the order of 0.5 to 1 m between the silt and peat samples with close modern analogues while the two samples from the top of the silt have poor modern analogues. We discuss further the evidence for potential sediment and diatom mixing in a later section.

The final earthquake horizon is the contact between a subsurface peat and intertidal sand that lies below the intertidal flat deposits that were uplifted in 1964 to become freshwater marsh behind the prominent pre-1964 dune ridge (Figure 6). Samples from two cores 2.5 km apart give minimum ages of 550 – 500 and 510 – 310 cal yr BP for coseismic uplift, followed by freshwater marsh developed on raised intertidal sediment surface, then relative sea-level rise and return to intertidal sedimentation in the tidal inlet seen on pre-1964 aerial photographs (Figure 6b).

In summary, the record at Katalla shows a complicated interaction of multiple earthquake cycles, with coseismic uplift and interseismic submergence, superimposed on coastal progradation and non-seismic sea-level change. The net effect of eustasy and glacio-isostasy is poorly understood for the area. While we see net relative uplift over the past 7000 years, from the mollusc bed (Figure 6), the silt-peat couplets at site 3.3 are much closer to the formation elevations we get from the transfer function estimates for peats at both Katalla and Copper River Delta, ~0.5 to 1m above MHHW.

Therefore net uplift over the last 2500 years is very small. In contrast, the peat-silt contact dated by minimum ages ~700 to 900 years ago at sites in three of the marshes (Figure 6) is well above the modern formation elevation, indicating recent net uplift. This may relate to a different seismic source for the most recent pre-1964 earthquake, recorded ~500 cal yr BP at sites in marsh 2, which we discuss further in the discussion section below.

3.3 Puffy Slough

Preliminary investigations of exposed sections and cores at Puffy Slough, an intertidal tidal marsh pre-1964, east of the Don Millar Hills and 2 to 5 km east of the Katalla sites, reveal >6 m of silt with up to three silt-peat couplets, all with sharp lower contacts and gradational upper contacts. These suggest at least three episodes of rapid uplift separated by gradual submergence (Figure 6d). With only seven cores taken across the marsh and low diatom counts in the silt units we simply note that the site appears to record a paleoseismic record with net submergence over multiple earthquake cycles, resulting from the combination of seismic and non-seismic land and sea-level change. The record at Puffy Slough contrasts with Katalla in at least two key respects. First, the absence of evidence for the earthquake and uplift recorded in marsh 2 at Katalla, dated ~500 cal yr BP. Second, the youngest pre-1964 couplet, mimimum age 760 – 670 cal yr BP, at Puffy Slough is at a lower elevation than the equivalent contact at Katalla, where it is at the base of the surface peat and not recording net submergence reverting to intertidal sedimentation.

4. QUANTIFYING COSEISMIC UPLIFT

Whereas coseismic subsidence may result in a peat-silt couplet, caused by submergence of freshwater marsh and rapid sedimentation of intertidal minerogenic deposits commencing hours to weeks after the earthquake (Atwater et al., 2001), peat formation on uplifted intertidal mudflat will not be instantaneous. There will be a time-lag before the colonization of the exposed sediment surface by terrestrial plant communities. Therefore, as noted above, we treat radiocarbon dates from the base of the peat as minimum ages for the earthquake. Diatom analyses across the silt-peat contacts from Katalla revealed a common phenomenon of mixed salinity assemblages in the upper part of the silt unit. In some cases it was limited to the single sample at the contact (Figure 7), but in others it extended further (Figure 8). At Katalla 5.5 we see a peak of *Tabellaria flocculosa* across the silt-peat contact, commencing ~4cm below the base of the peat. *T. flocculosa* is a freshwater species most commonly found attached to the submerged stems of littoral species of sedges and reeds (Knudson, 1954; Patrick and Reimer, 1966). We interpret this as evidence of ponding of freshwater on the surface of the uplifted tidal flat, now above the limit of tidal inundation. Diatoms can colonise and grow within a few weeks, therefore reflecting the environment following uplift but before colonization by terrestrial plants. During this time we may expect redistribution of surface sediment by a variety of processes, including rain, wind, surface water flow and winter ice freeze-thaw. Where this occurs the redeposited silt with freshwater diatoms does not represent the pre-earthquake environment and elevation. At Katalla 5.5 low diatom counts prevent us taking this analysis further but it may be that

the base of the visibly coarser layer at 102 cm (Figure 8 and 9) is the earthquake horizon, overlain by 5 cm of reworked silt with mix of diatoms from two main sources; those already in the silt and those growing during the period of sediment reworking and deposition. We have seen comparable evidence for similar sequences of events between the time of uplift and peat formation at other sites. Figure 10c shows a box sample from a tidal exposure at Copper River Delta that we declined to analyse further as we could not trace the lateral continuity of the coarse layer more than a few meters in the time available during the fieldwork. Mixed diatom assemblages below the modern peat on the marsh at Cape Suckling uplifted in 1964 (Shennan, 2009) may also be the result of sediment reworking on the uplifted surface prior to peat growth.

In summary, up to four factors may combine to make it probable that reconstructions based on sediment and diatom stratigraphies will give minimum estimates of both the age of a Holocene earthquake and the amount of coseismic uplift. First, there is the time interval between uplift and peat accumulation. Second, there may be sediment reworking at the top of the silt unit so it may be difficult to establish the pre earthquake paleo surface elevation; mixing of tidal flat and purely freshwater diatom communities would produce a too high estimate. Third, there will be initially rapid post-seismic subsidence during the time interval between uplift and peat accumulation. For example, at Cordova, only a few kilometers west of Copper River Delta, following uplift in 1964, the tide gauge shows ~20 cm sea-level rise 1964 to 1979 and ~ 5 cm further rise 1979 to 2012 (NOAA, 2013). Finally, ground shaking of the unconsolidated tidal flat sediment

column during the earthquake may cause compaction and dewatering of unconsolidated sediment and surface lowering.

5. AGE MODELLING

The OxCal Bayesian modeling approach outlined by Bronk Ramsey and Lienkaemper (Bronk Ramsey, 2009; Lienkaemper and Bronk Ramsey, 2009) determines the best-fit ages and recurrence intervals of multiple great earthquakes. It allows us to combine the ages on earthquake horizons from all sites across the Prince William Sound segment, whether they record coseismic uplift or coseismic subsidence. This a fundamental difference to previous studies which first determine the chronology at each site, then compare the patterns between sites (Carver and Plafker, 2008; Shennan and Hamilton, 2006).

This new approach assumes that the dated indicators of uplift or subsidence are either minimum or maximum ages on the earthquake horizon. For coseismic subsidence, maximum ages come from a peat contact below an intertidal silt unit and minimum ages from samples within the silt unit. For coseismic uplift, maximum ages come from the top part of intertidal silt below peat, and minimum ages from the peat (e.g. Figures 4 and 6).

Previous studies from Cook Inlet demonstrated the potential of contamination of bulk peat samples by older carbon, such as coal deposits in the catchment (Hamilton et al., 2005), so we exclude bulk peat samples from that area. With many bulk peat dates available for other areas, particularly the key record from Copper River Delta published

299 previously (Carver and Plafker, 2008) we compared ages using bulk peat and AMS
300 dated samples on in situ plant macrofossils from the same locations. Whereas we see
301 major differences in the ages of the paired samples for sites around Cook Inlet we find
302 no significant differences for the four from Copper River Delta (Figure 10). Therefore
303 we include bulk peat ages from Copper River Delta in our analysis, but only ages for
304 samples of macrofossils at all other sites.
305
306 The OxCal Bayesian model seeks to estimate the age of each earthquake that is
307 bracketed by dated samples assuming no knowledge of sedimentation rate pre- or post-
308 earthquake. Samples are grouped into "*phases*", where one *phase* is all the samples
309 giving a minimum age on earthquake *n*, and another *phase* will be all the maximum
310 ages for earthquake *n* (Lienkaemper and Bronk Ramsey, 2009). There is no
311 chronological ordering within a *phase*, but the stratigraphic ordering of phases and
312 earthquake horizons is a powerful constraint (Figure 11a). Our full model uses 9 pre-
313 historic earthquakes of unknown age and the 1964 earthquake as a known boundary.
314 We exclude the ~ 500 cal yr BP earthquakes at Kodiak and Katalla as we have no
315 evidence for them rupturing other parts of the 1964 rupture zone. Between each pair of
316 earthquakes we have two *phases*, assuming the *phase* of minimum ages for the older
317 earthquake occurs before the *phase* of maximum ages for the younger earthquake
318 (Figure 11a). OxCal provides graphical output (Figure 11b) of the modeled probability
319 density functions for each sample along with the likelihood distribution from the
320 radiocarbon measurement, and the probability density function of each earthquake age

and interval between earthquakes, which we summarise with the mean and 95.5% probability range (Table 3).

6. EARTHQUAKE AGES AND RECURRENCE

The OxCal Bayesian model gives the age of the penultimate great earthquake as 870 ± 34 BP (2σ) with decreasing precision for each older earthquake (Figure 12a and Table 3)). This is a function of both the number of samples available, in part reflecting the limits to coring depth, and the number of sites which record the earthquake. We do not consider further the oldest three earthquakes (not shown in figure 12) as they are only constrained by samples from one site (Copper River Delta) and the precision of the estimated ages is poor, ± 180 to ± 300 years.

The mean recurrence interval for the seven earthquakes from EQ6, ~3550 cal yr BP, to 1964 is ~595 years. This average is heavily influenced by the relatively long interval, 883 ± 34 (2σ) years, between the EQ1 and 1964, compared to the intervals between the older earthquakes (Figure 12b). The pre-1964 earthquakes have recurrence intervals that range from ~420 to ~610 years, with a mean ~535. While it would be preferable to have more samples from more sites for EQ5 and EQ6 in order to better constrain their ages and interval, it seems clear that the interval between the penultimate great earthquake and 1964 is the longest recorded.

7. DISCUSSION AND CONCLUSIONS

Is the 1964 earthquake typical of other Late Holocene great earthquakes? In terms of coastal stratigraphy we certainly see comparable sediments and biostratigraphy, but in addition to the temporal variations discussed above, there are also spatial differences in the paleoseismic record (Carver and Plafker, 2008; Hamilton and Shennan, 2005b; Shennan and Hamilton, 2006). For example, the coseismic uplift recorded east of Cape Yakataga correlates with the penultimate earthquake at numerous other sites (Figure 13), and may indicate a greater area of rupture than in 1964 (Shennan et al., 2009) yet there is no evidence of coseismic subsidence at Kenai and Kasilof, on the Cook Inlet shore of the Kenai Peninsula (Shennan and Hamilton, 2006) (Figure 1). The Kenai record, along with archaeological evidence, led Hutchinson and Crowell (2007) to suggest that the 1964 rupture zone comprises three segments that may not always rupture together: Kodiak, Kenai and Prince William Sound.

It is critical to note that the longest and most comprehensive records all come from the Prince William Sound segment and the area of flat slab subduction of the Yakutat microplate (Figures 1 and 13) and at this stage we can draw three main conclusions with respect to this region. First, multiple earthquake cycles over at least the past 4000 years in the Prince William Sound segment follow the same general pattern of co-seismic uplift and subsidence as 1964 yet show net subsidence over this period at most sites. To separate the effects of glacial isostatic adjustment, eustasy and interseismic tectonic motions will require expansion of existing modeling approaches (Barlow et al., 2012). Glacio-isostasy and eustasy produce differences in relative land and sea levels

366 that occur gradually through time and over distances on the order of 10s to 100s of
367 kilometers.
368
369 In contrast, we observe measurable differences in net motion over shorter distances, for
370 example, between Katalla and Puffy Slough, Katalla and Copper River Delta, described
371 above, and between the Suckling Hills/Cape Suckling and the marsh immediately to the
372 west, discussed by Shennan (2009). Therefore we consider the possibility of upper
373 plate faulting and slip on the megathrust contributing to these differences over short
374 distances, superimposed on the broader scale effects of glacio-isostasy (Barlow et al.,
375 2012; Shennan and Hamilton, 2010).
376
377 A schematic cross section of the plate boundary from Cook Inlet to the Malaspina
378 Glacier places the paleoseismic sites in a structural framework relative to the Aleutian
379 megathrust and either known or inferred upper plate faults (Figure 13). Accretion of the
380 upper crustal section of the Yakutat microplate begins at the Malaspina Glacier and
381 extends to the Ragged Mountain fault in the west. The upper plate is imbricated by
382 several faults with Holocene displacement. These include the Hanning and Patton Bay
383 faults at Montague Island which ruptured beneath Prince William Sound in 1964, the
384 Ragged Mountain fault at Katalla, the Cape Suckling – Bering Glacier fault, and several
385 faults located in the vicinity of Icy Bay and the Malaspina Glacier.
386
387 The pattern of regional surface displacement and upper crustal faulting during the 1964
388 earthquake provides some insight into viable hypotheses for contributing to net

Holocene uplift of at least 4 m at Katalla, and similar amounts indicated by mid-Holocene marine molluscs at Bering Glacier (Shennan, 2009) and Cape Suckling (Plafker and Rubin, 1967). Rupturing of the Prince William Sound segment of the megathrust extended from beneath the southeastern edge of Cook Inlet to the Bering Glacier region, whilst upper plate faulting propagated to the surface on the Hanning and Patton Bay faults within Prince William Sound (Figure 13; Plafker, 1969). There was no surface faulting at Cape Suckling, although a spike in uplift suggests reverse motion on the Suckling Hills – Bering Glacier fault that was confined to the subsurface. There is no evidence for surface faulting at Ragged Mountain in 1964.

We infer a local earthquake beneath Katalla that caused uplift ~500 cal yr BP and was followed by interseismic subsidence prior to uplift of the coast in 1964. Does the former event reflect blind reverse faulting beneath the Katalla Valley that is temporally decoupled from great megathrust earthquakes? Certainly the structural setting of the valley is amendable to the presence of a blind thrust given the complexly folded and faulted rocks mapped at the surface (Winkler and Plafker, 1993) and evidence for duplex thrust faulting where roof and floor thrusts cause doubling up of the crustal section (Pavlis et al., 2012). Furthermore, modeling of GPS geodetic data shows that the valley is part of a small tectonic block that is currently deforming and rotating separately relative to the regions east of the Bering Glacier and west of Ragged Mountain (Elliott, 2011).

We consider two hypotheses for faulting contributing to net Holocene uplift at Katalla, the first focuses solely on the history of rupturing on the megathrust, the second invokes uplift driven by a blind fault beneath the valley. We prefer the second hypothesis, but cannot discount the first given the circumstantial nature of the paleoseismic and geologic data.

Hypothesis 1: The megathrust beneath Katalla is subject to large earthquakes from time to time that do not rupture the entire Prince William Sound segment. This is certainly plausible given the expected heterogeneity of the megathrust interface near the western edge of Yakutat microplate accretion. The ~500 cal yr BP uplift at Katalla may be such an event, if so, it reversed the pattern of interseismic subsidence following the penultimate great earthquake, that is, the great earthquake ~870 cal yr BP. If localized uplift beneath the valley is repeated from time to time independent of great earthquakes on the Prince William Sound segment then a modest amount of net uplift could accumulate, contributing to the 4+ m over 7000 years. The primary problem with this hypothesis is that we have found no evidence within cores for older events like that of ~500 cal yr BP. All the other silt-peat couplets that indicate coseismic uplift at Katalla correlate with similar horizons at Copper River Delta, Puffy Slough and the marshes west of Cape Suckling over the last 2600 years. This implies a return period for localized slip that is greater than 2100 years, a recurrence period that is of course, common (Wesson et al., 2008) on upper plate faults that operate independent of the megathrust for much of their history.

Hypothesis 2: There is a blind reverse fault beneath Katalla Valley, with a long recurrence interval, which contributed to net uplift of 4+ m in the last 7000 years, even though coseismic uplift in great megathrust earthquakes was followed by interseismic subsidence. This hypothesis has the following merits: 1) the blind reverse fault model is consistent with net uplift at Katalla but net subsidence at Copper River Delta and Puffy Slough; 2) similar net uplift at Cape Suckling and Bering Glacier is explained by activation of the Suckling Hills – Bering Glacier upper plate fault (Chapman et al., 2011), with net subsidence in the marshes to the west, including Puffy Slough. 3) The blind fault model is consistent with the complex structural geology (Bruhn et al., 2004; Pavlis et al., 2012; Winkler and Plafker, 1993); T.L. Pavlis, personal communications, 2013) surrounding and inferred to underlie the Katalla Valley.

Therefore our second conclusion is that contributions to net uplift may occur by both slip on the megathrust and upper plate faulting (Figure 13), the latter leading to measurable differences in coseismic uplift over a few kilometers.

Thirdly, the long interval between the penultimate and 1964 earthquake appears unusual given the paleoseismic record for the last several thousand years. The reason for this difference is uncertain given the available data. One possibility is that the long return period simply reflects part of the natural variability in the time dependent behavior of the megathrust. Another, is that the two events ~500 cal yr BP, one at Kodiak and the other in the vicinity of Katalla, reduced the level of stress on the megathrust and retarded rupturing across the whole area until 1964. The nature of the ~500 cal yr BP

events remains uncertain - slip on the megathrust is inferred by Carver and Plafker (2008) at Kodiak, while imbricate faulting within the crust above the megathrust seems more likely at Katalla. Whether it was it was a slipping patch on the megathrust or an upper plate fault at Katalla, the Katalla and Kodiak events would have reduced stress in those two regions, and possibly initiated creep, and hence time-dependent stress release, on the megathrust beneath Prince William Sound, delaying the onset of seismic rupturing until 1964?

One of the changes made in the 2007 modification to the seismic hazard maps for Alaska was to change the assumed recurrence interval of great earthquakes in the Prince William sound segment from 750 to 650 years, based upon the paleoseismic research published at the time (Wesson et al., 2007). Although this made little change to the hazard for most locations, enhancement of the paleoseismic records provides better characterization of the megathrust and upper plate faults and therefore a more satisfactory justification in terms of observation and understanding for calculating seismic hazard. The age modeling results described above provide more reliable and precise estimates of earthquake recurrence and could contribute to enhancements of both time-dependent and time-independent seismic hazard analyses for Alaska. A further enhancement would be to include the Katalla area as a source of seismic hazard, similar to other locations in the western part of the Yakutat microplate, such as the two M_w8+ ruptures in 1899 (Plafker and Thatcher, 2008).

ACKNOWLEDGMENTS

Sarah Cervera Heinlein, Peter Haeussler and Rich Koehler for help in the field; Christopher Bronk Ramsey for guidance on Oxcal modeling; Gary Carver, George Plafker and Terry Pavlis for discussions and comments concerning paleoseismology and tectonics. This work is supported by the Saint Elias Erosion and Tectonics project (STEEP), NSF 0408959, the U.S. Geological Survey, Department of the Interior, earthquake hazards projects awards 06HQGR0033, G09AP00105 and G10AP00075 (The views and conclusions contained in this document are those of the authors and should not be interpreted as necessarily representing the official policies, either expressed or implied, of the U.S. Government) and NERC Radiocarbon Facility (grants #935.0901 and #1339.1008). This work forms a contribution to IGCP Project 588 "Preparing for Coastal Change".

REFERENCES

Atwater, B.F., Yamaguchi, D.K., Bondevik, S., Barnhardt, W.A., Amidon, L.J., Benson, B.E., Skjerdal, G., Shulene, J.A., and Nanayama, F., 2001, Rapid resetting of an estuarine recorder of the 1964 Alaska earthquake: Geological Society of America Bulletin, v. 113, p. 1193-1204.

Barlow, N.L.M., Shennan, I., and Long, A.J., 2012, Relative sea-level response to Little Ice Age ice mass change in south central Alaska: Reconciling model predictions and geological evidence: Earth and Planetary Science Letters, v. 315-316, p. 62-75.

Boyd, O.S., Zeng, Y., Bufe, C.G., Wesson, R.L., Pollitz, F., and Hardebeck, J.L., 2008, Toward a time-dependent probabilistic seismic hazard analysis for Alaska, *in* Freymueller, J.T., Haeussler, P.J., Wesson, R., and Ekström, G., eds., Active Tectonics and Seismic Potential of Alaska, Volume 179: Geophysical Monograph Series: Washington, DC, AGU, p. 399-416.

Bronk Ramsey, C., 2009, Bayesian analysis of radiocarbon dates: Radiocarbon, v. 51, p. 337-360.

Bruhn, R.L., Pavlis, T.L., Plafker, G., and Serpa, L., 2004, Deformation during terrane accretion in the Saint Elias orogen, Alaska: Geological Society of America Bulletin, v. 116, p. 771-787.

Carver, G., and Plafker, G., 2008, Paleoseismicity and Neotectonics of the Aleutian Subduction Zone - An Overview, *in* Freymueller, J.T., Haeussler, P.J., Wesson, R., and Ekstrom, G., eds., Active tectonics and seismic potential of Alaska: Geophysical Monograph Series: Washington, American Geophysical Union, p. 43-63.

Chapman, J.B., Worthington, L.L., Pavlis, T.L., Bruhn, R.L., and Gulick, S.P., 2011, The Suckling Hills Fault, Kayak Island Zone, and accretion of the Yakutat microplate, Alaska: Tectonics, v. 30, p. TC6011, doi:10.1029/2011TC002945.

Elliott, J., 2011, Active Tectonics in Southern Alaska and the role of the Yakutat Block constrained by GPS measurements: Fairbanks, University of Alaska Fairbanks.

Hamilton, S., and Shennan, I., 2005, Late Holocene relative sea-level changes and the earthquake deformation cycle around upper Cook Inlet, Alaska: Quaternary Science Reviews, v. 24, p. 1479-1498.

Hamilton, S., Shennan, I., Combellick, R., Mulholland, J., and Noble, C., 2005, Evidence for two great earthquakes at Anchorage, Alaska and implications for multiple great earthquakes through the Holocene: Quaternary Science Reviews, v. 24, p. 2050-2068.

Hutchinson, I., and Crowell, A.L., 2007, Recurrence and Extent of Great Earthquakes in Southern Alaska During the Late Holocene from an Analysis of the Radiocarbon Record of Land-Level Change and Village Abandonment: Radiocarbon, v. 49, p. 1323-1385.

Knudson, B.M., 1954, The Ecology of the Diatom Genus Tabellaria in the English Lake District: Journal of Ecology, v. 42, p. 345-358.

Lienkaemper, J.J., and Bronk Ramsey, C., 2009, OxCal: Versatile tool for developing paleoearthquake chronolgies - A primer: Seismological Research Letters, v. 80, p. 431-434.

McCalpin, J., P, and Carver, G., 2009, Paleoseismology of compressional tectonic environments, *in* McCalpin, J., P, ed., Paleosismology, Volume 95: International Geophysics Series: Burlington, Academic Press, p. 315 - 419.

Nelson, A.R., Shennan, I., and Long, A.J., 1996, Identifying coseismic subsidence in tidal-wetland stratigraphic sequences at the Cascadia subduction zone of western North America: Journal of Geophysical Research, v. 101, p. 6115-6135.

NOAA, 2013, http://tidesandcurrents.noaa.gov/sltrends/index.shtml Accessed August 1, 2013.

Patrick, R., and Reimer, C.W., 1966, The Diatoms of the United States. Volume 1. Monographs of The Academy of Natural Sciences of Philadelphia No 13: Philadelphia, Academy of Natural Sciences of Philadelphia, 688 p.

Pavlis, T.L., Chapman, J.B., Bruhn, R.L., Ridgway, K., Worthington, L.L., Gulick, S.P.S., and Spotila, J., 2012, Structure of the actively deforming fold-thrust belt of the St. Elias orogen with implications for glacial exhumation and three-dimensional tectonic processes: Geosphere, v. 8, p. 991-1019.

Plafker, G., 1969, Tectonics of the March 27, 1964, Alaska earthquake: U.S. Geological Survey Professional Paper, v. 543-I, p. 74.

—, 1987, Regional geology and petroleum potential of the northern Gulf of Alaska continental margin, *in* Scholl, D.W., Grantz, A., and Vedder, J.G., eds., Geology and Resource Potential of the Continental Margin of Western North America and Adjacent Ocean Basins - Beaufort Sea to Baja California, Volume 6: Earth Science Series: Houston, Circum-Pacific Council for Energy and Mineral Resources, p. 229-268.

Plafker, G., Lajoie, K.R., and Rubin, M., 1992, Determining intervals of great subduction zone earthquakes in southern Alaska by radiocarbon dating, *in* Taylor, R.E.,

Long, A., and Kra, R.S., eds., Radiocarbon after four decades. An interdisciplinary perspective: New York, Springer Verlag, p. 436-452.

Plafker, G., and Rubin, M., 1967, Vertical tectonic displacements in south central Alaska during and prior to the great 1964 earthquake: Journal of Geoscience, v. 10, p. 1-7.

Plafker, G., and Thatcher, W., 2008, Geological and geophysical evaluation of the mechanisms of the Great 1899 Yakutat Bay Earthquakes, *in* Freymueller, J.T., Haeussler, P.J., Wesson, R., and Ekström, G., eds., Active Tectonics and Seismic Potential of Alaska, Volume 179: Geophysical Monograph Series: Washington, DC, AGU, p. 215-236.

Richards, S.W., 2000, Holocene history of the Katalla River Valley, Alaska: Salt Lake City, Univeristy of Utah.

Shennan, I., 2009, Late Quaternary sea-level changes and palaeoseismology of the Bering Glacier region, Alaska: Quaternary Science Reviews, v. 28, p. 1762-1773.

Shennan, I., Bruhn, R., and Plafker, G., 2009, Multi-segment earthquakes and tsunami potential of the Aleutian megathrust: Quaternary Science Reviews, v. 28, p. 7-13.

Shennan, I., and Hamilton, S., 2006, Coseismic and pre-seismic subsidence associated with great earthquakes in Alaska: Quaternary Science Reviews, v. 25, p. 1-8.

Shennan, I., and Hamilton, S.L., 2010, Holocene sea-level changes and earthquakes around Bering Glacier, *in* Shuchman, R., Josberger, E., and Jenkins, L., eds., Bering Glacier: Interdisciplinary studies of Earth's largest temperate surging glacier: Geological Society of America Special Paper 462: Boulder, Geological Society of America, p. 275 - 290

Sirkin, L., and Tuthill, S.J., 1971, Late Pleistocene palynology and stratigraphy of Controller Bay region, Alaska, *in* Ters, M., ed., Études sur le quaternaire dans le monde : VIIIe Congrès INQUA, Paris, 1969, Volume 1: Paris, Centre National de la Recherche Scientifique, p. 197-208.

Tysdal, R.G., Hudson, T., and Plafker, G., 1976, Surface features and recent movement along the Ragged Mountain fault, south-central Alaska, U.S. Geological Survey Miscellaneous Field Studies Map MF-782, 1 sheet, scale 1:24000.

Watcham, E.P., Shennan, I., and Barlow, N.L.M., 2013, Scale considerations in using diatoms as indicators of sea-level change: lessons from Alaska: Journal of Quaternary Science, v. 28, p. 165-179.

Wesson, R.L., Boyd, O.S., Mueller, C.S., Bufe, C.G., Frankel, A.D., and Petersen, M.D., 2007, Revision of time-independent probabilistic seismic hazard maps for Alaska, U.S. Geological Survey Open-File Report, Volume 2007-1043, p. 1-33.

Wesson, R.L., Boyd, O.S., Mueller, C.S., and Frankel, A.D., 2008, Challenges in making a seismic hazard map for Alaska and the Aleutians, *in* Freymueller, J.T., Haeussler, P.J., Wesson, R., and Ekström, G., eds., Active Tectonics and Seismic Potential of Alaska, Volume 179: Geophysical Monograph Series: Washington, DC, AGU, p. 385-397.

Winkler, G.R., and Plafker, G., 1993, Geologic map of the Cordova and Middleton Island quadrangles, Southern Alaska, U.S. Geological Survey Miscellaneous Investigations Series Map 1984, 1 sheet, scale 1:250,000., U.S. Geological Survey.

FIGURE CAPTIONS

Figure 1: Tectonic setting of south central Alaska. Approximate area of coseismic subsidence (light grey) and uplift (dark grey) in 1964 and the western segment of the Yakutat microplate (dotted). Extent of subducted Yakutat slab shown to 50 km depth. Star symbols indicate epicentre of two M_w8+ earthquakes in 1899. Note that Hutchinson and Crowell (2007) adopt a further subdivision, with the Prince William Sound segment partitioned into two, distinguishing a Kenai segment, the part beneath the Kenai Peninsula not underlain by the subducted Yakutat slab.

Figure 2: LANDSAT image, 2013, of the coastal setting of the new field sites.

Figure 3: Copper River Delta: exposure of two silt-peat couplets at location 3 discussed in the text; coring revealed a third couplet.

Figure 4: Copper River Delta - Alaganik Slough sampling locations; a) 2013 LANDSAT image; b) air photo, August 1952; c) summary stratigraphy at sample locations, black = peat, adjacent triangle = sharp contact, white = silt, tree root symbol where present, calibrated age 95% age ranges BP (details in table 2); d) summary diatom diagram showing species accounting for >10% in at least one sample, and summary salinity classes, depths in cm relative to silt-peat contact.

Figure 5: Copper River Delta, mean and 95% uncertainty model estimates of paleo marsh surface elevation change across silt-peat couplets using the diatom-based transfer function method described in the text.

Figure 6: a) LANDSAT image of Katalla River Valley and Puffy Slough, with marshes numbered and individual sample locations indicated by white circles ; b) air photo mosaic of the area, August 1950. Note the extent of tidal inundation and difference in vegetation extent, c) Katalla River summary stratigraphy and geomorphology along

transect X′ - X, black = peat, white = silt, stipple = sand (top contacts of all silt and sand units shown are sharp) and calibrated age 95% age ranges cal yr BP (details in table 2); d) Puffy Slough, example of a core recording four episodes of coseismic uplift (the base of the surface peat represents uplift in 1964) superimposed upon net submergence.

Figure 7: Katalla site 3.10 summary diatom diagram and reconstruction estimates of paleo surface marsh elevations with 95% confidence limits: showing species accounting for >10% in at least one sample, total count per sample, radiocarbon ages cal yr BP and summary salinity classes, depths in cm relative to present ground surface; for elevation reconstructions, diamond symbol indicates low count, 125 diatoms, all others shown are based on >200. Grey symbol fill indicates close modern analogue, white indicates poor modern analogue.

Figure 8: Katalla site 5.5 summary diatom diagram and photograph of box sample across the contact, showing species accounting for >10% in at least one sample, total count per sample, and summary salinity classes, depths in cm relative to present ground surface.

Figure 9: a) marsh stratigraphy exposed along Katalla River, at site 5.5; b) 25 cm box section sampled across the contact at site 5.5; c) box sample across silt-peat contact, showing sand layer within the silt unit, sample taken near to Copper River Delta site 3.

Figure 10: Comparison of radiocarbon ages on paired samples of bulk peat and herbaceous macrofossils.

Figure 11: Age model of earthquake recurrence, a – Oxcal model structure of phases for constraining earthquake ages (Lienkaemper and Bronk Ramsey (2009) ; b – example of model input and output, for just EQ 1. The full model repeats this for each earthquake. Input:for each sample within a phase the calibrated age, in grey. Outputs in black, the probability density function from Bayesian modelling for each input sample and the 95.4% probability age of the intervening earthquake.

Figure 12: Probability density functions for earthquake ages (a) and intervals (b).

Figure 13: .Schematic cross section of the plate boundary from Cook Inlet to the Malaspina Glacier, with summary of major earthquakes, direction of coseismic deformation and net Holocene motion: grey = no data of that age, ⇧ uplift , ⬇ subsidence, ▭ no deformation. Large crustal faults are either known from surface offsets or inferred from paleoseismology and/or geologic mapping. The Ragged Mountain fault is a thrust fault that sutures the Yakutat terrane to the Early Tertiary Alaskan plate margin. That fault is marked by a 30 km-long system of Quaternary normal fault scarps that may reflect reactivation in extension (Tysdal et al., 1976), or possibly flexure above the tip of a buried thrust fault. The faults between Ragged Mountain and the Suckling Hills are inferred blind thrust faults within a complicated stack of imbricate thrusts that form an anticline beneath the Katalla Valley, but may have little or no surface manifestation other than uplift in the valley. The faults are inferred from geologic mapping (T.L. Pavlis, personal communications, 2013) and local uplift in the valley ~500 cal yr BP as discussed in section 7. The Suckling Hills and Bering Glacier faults are part of the same fault system that link to the Kayak Island Zone offshore (Chapman et al., 2011). The fault beneath Icy Bay is the Malaspina thrust fault which is known from both drill hole data (Chapman et al., 2011; Plafker, 1987) and geodetic observations (e.g. (Elliott, 2011).

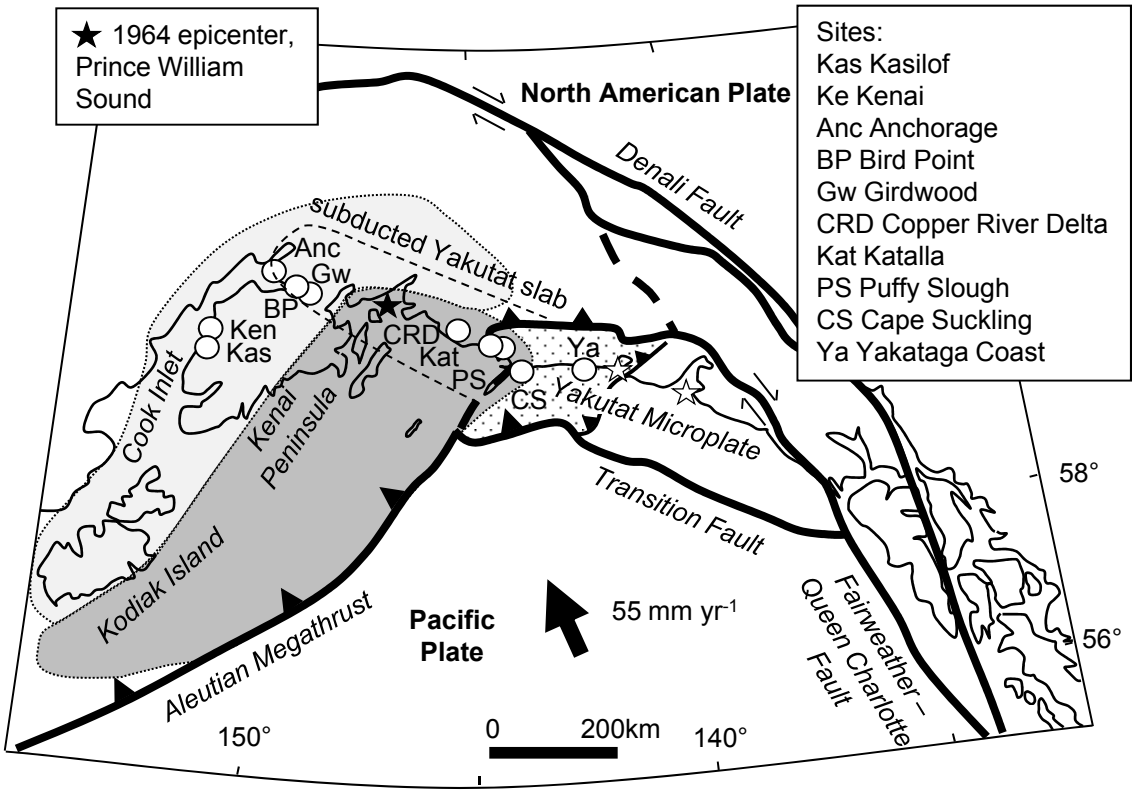
★ 1964 epicenter, Prince William Sound
Sites:
Kas Kasilof
Ke Kenai
Anc Anchorage
BP Bird Point
Gw Girdwood
CRD Copper River Delta
Kat Katalla
PS Puffy Slough
CS Cape Suckling
Ya Yakataga Coast
North American Plate
Denali Fault
subducted Yakutat slab
Anc
Gw
BP
Ken
Kas
CRD
Kat
PS
CS
Ya
Yakutat Microplate
Transition Fault
Cook Inlet
Kenai Peninsula
Kodiak Island
Aleutian Megathrust
Pacific Plate
55 mm yr-1
Fairweather – Queen Charlotte Fault
58°
56°
150°
140°
0
200km

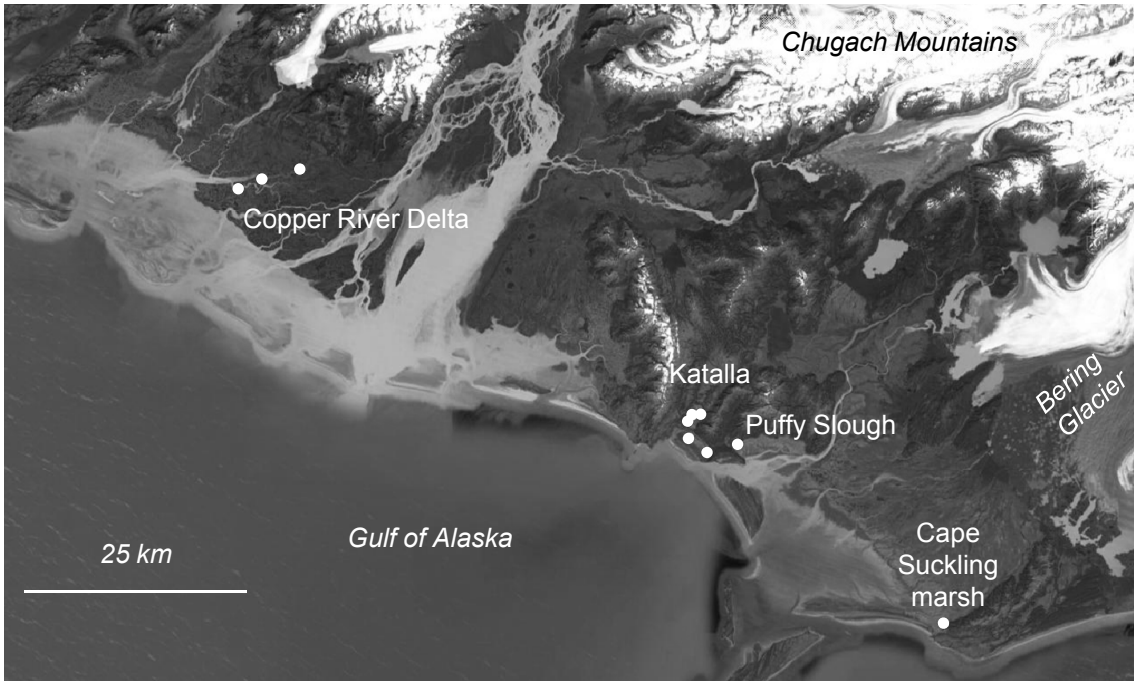
Chugach Mountains
Copper River Delta
Katalla
Puffy Slough
Bering Glacier
Gulf of Alaska
25 km
Cape Suckling marsh

Depth below surface of modern high marsh
~0.50 m

~1.25 m

~2.70 m

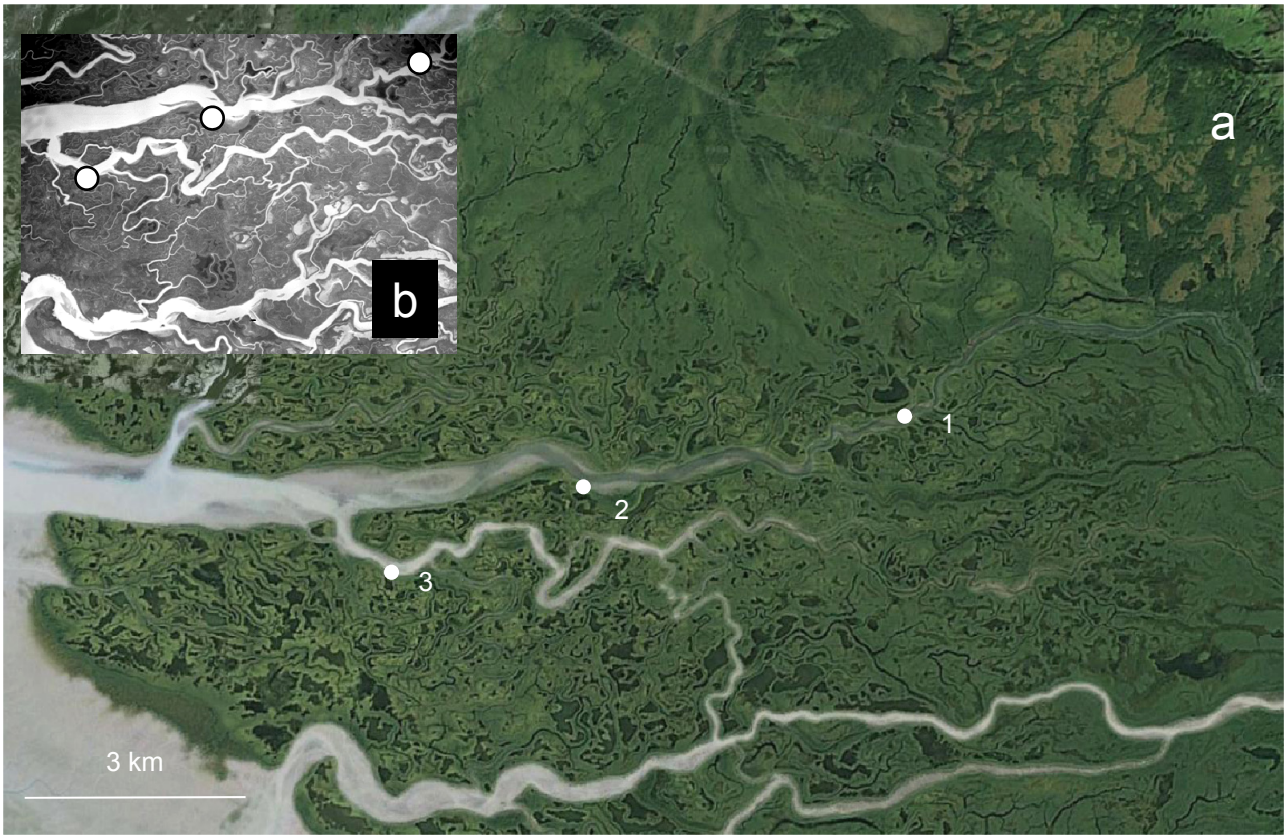
a
b
1
2
3
3 km

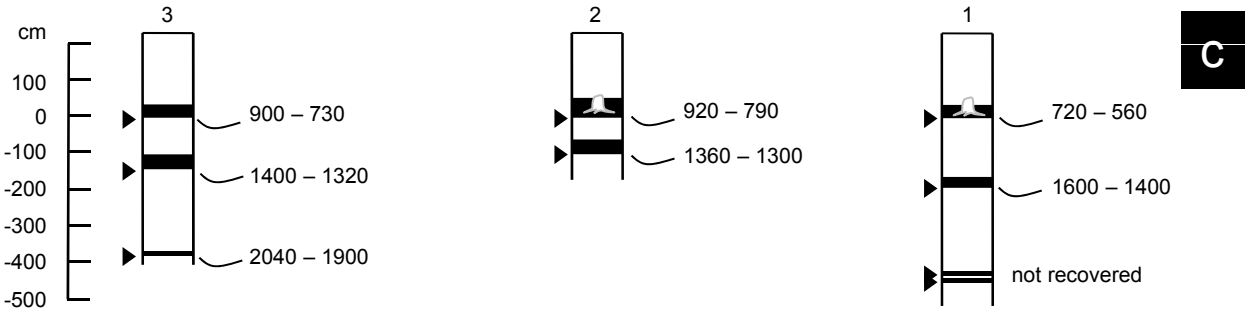
3
2
1
cm
100
0
-100
-200
-300
-400
-500
900 – 730
1400 – 1320
2040 – 1900
920 – 790
1360 – 1300
720 – 560
1600 – 1400
not recovered
c

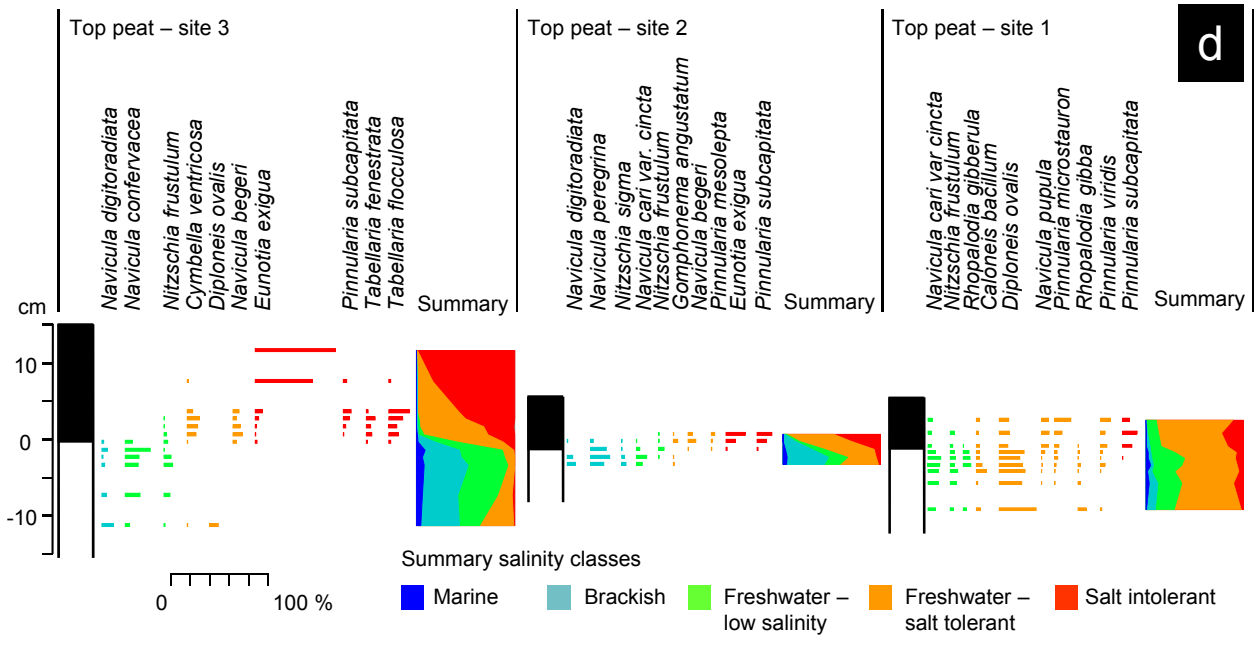
Top peat – site 3
Navicula digitoradiata
Navicula confervacea
Nitzschia frustulum
Cymbella ventricosa
Diploneis ovalis
Navicula begeri
Eunotia exigua
Pinnularia subcapitata
Tabellaria fenestrata
Tabellaria flocculosa
Summary
Top peat – site 2
Navicula digitoradiata
Navicula peregrina
Nitzschia sigma
Navicula cari var. cincta
Nitzschia frustulum
Gomphonema angustatum
Navicula begeri
Pinnularia mesolepta
Eunotia exigua
Pinnularia subcapitata
Summary
Top peat – site 1
Navicula cari var cincta
Nitzschia frustulum
Rhopalodia gibberula
Caloneis bacillum
Diploneis ovalis
Navicula pupula
Pinnularia microstauron
Rhopalodia gibba
Pinnularia viridis
Pinnularia subcapitata
Summary
d
cm
10
0
-10
0
100 %
Summary salinity classes
Marine
Brackish
Freshwater – low salinity
Freshwater – salt tolerant
Salt intolerant

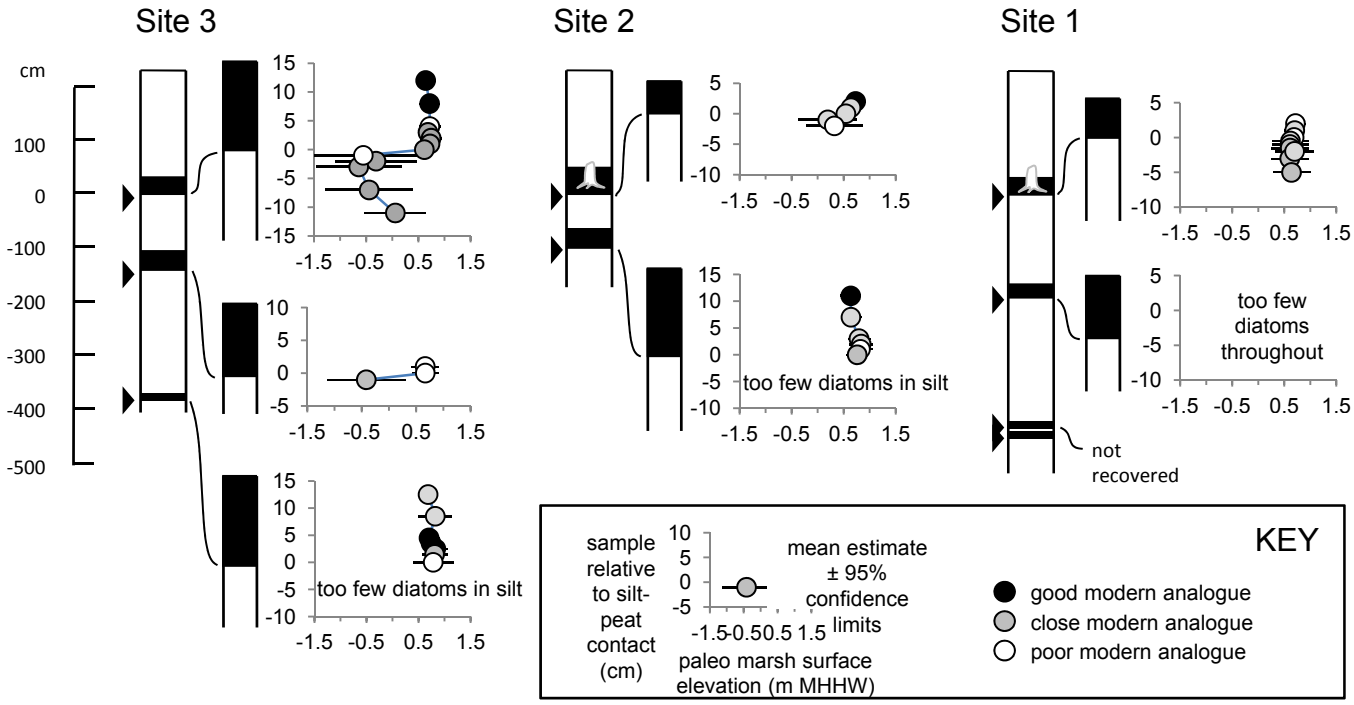
Site 3
Site 2
Site 1
cm
100
0
-100
-200
-300
-400
-500
too few diatoms in silt
too few diatoms in silt
too few diatoms throughout
not recovered
sample relative to silt-peat contact (cm)
mean estimate ± 95% confidence limits
paleo marsh surface elevation (m MHHW)
KEY
good modern analogue
close modern analogue
poor modern analogue

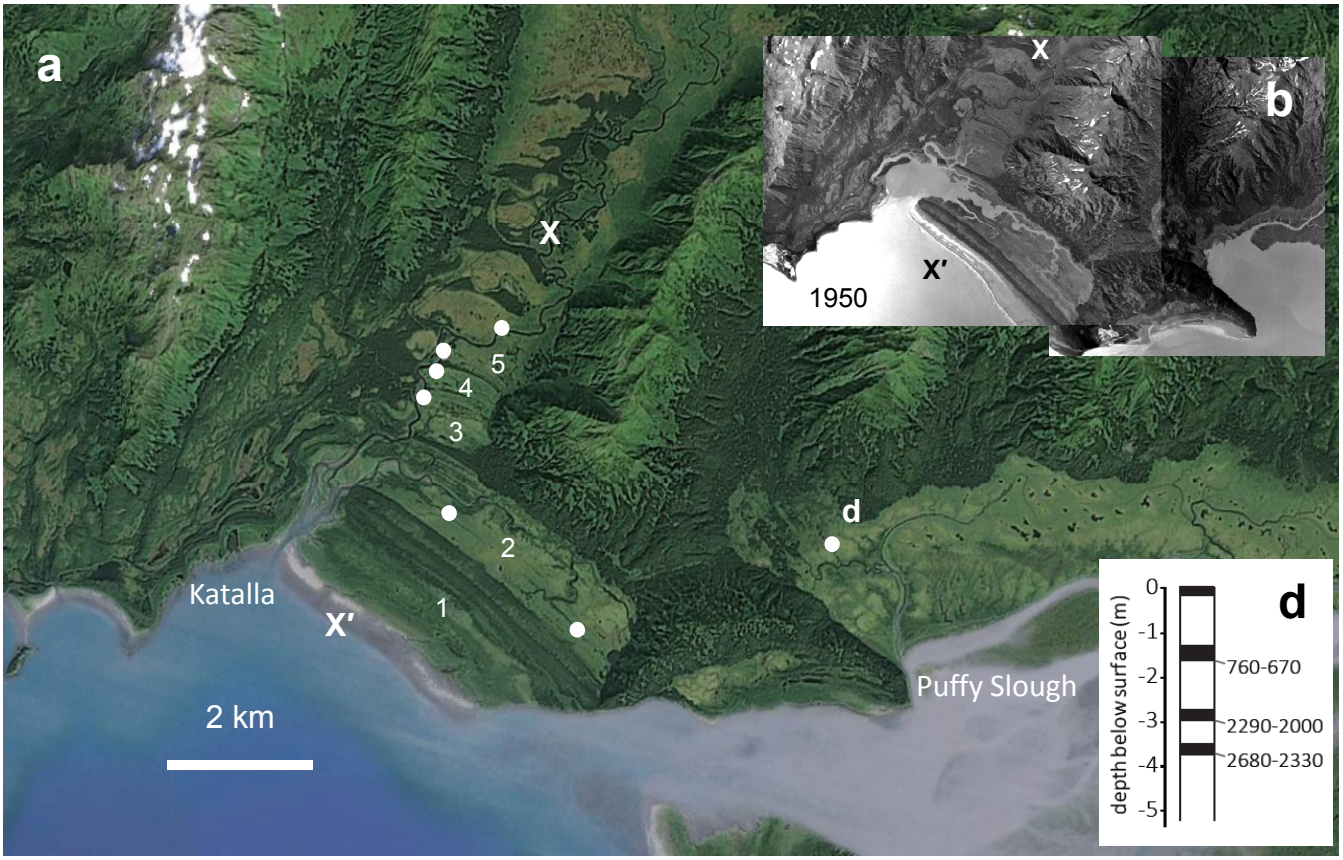
a
X
X'
1
2
3
4
5
d
Katalla
2 km
Puffy Slough
b
1950
d
depth below surface (m)
0
-1
-2
-3
-4
-5
760-670
2290-2000
2680-2330

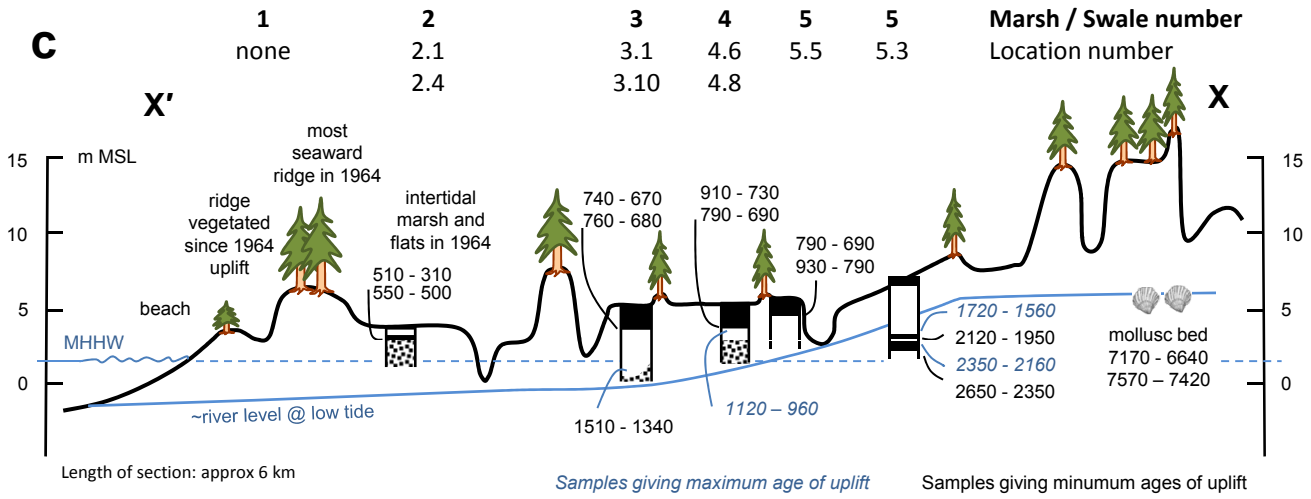
c
X'
X
1
none
2
2.1
2.4
3
3.1
3.10
4
4.6
4.8
5
5.5
5
5.3
Marsh / Swale number
Location number
15
10
5
0
m MSL
most seaward ridge in 1964
ridge vegetated since 1964 uplift
beach
MHHW
intertidal marsh and flats in 1964
510 - 310
550 - 500
740 - 670
760 - 680
910 - 730
790 - 690
790 - 690
930 - 790
~river level @ low tide
1510 - 1340
1120 – 960
1720 - 1560
2120 - 1950
2350 - 2160
2650 - 2350
mollusc bed
7170 - 6640
7570 – 7420
Length of section: approx 6 km
Samples giving maximum age of uplift
Samples giving minumum ages of uplift

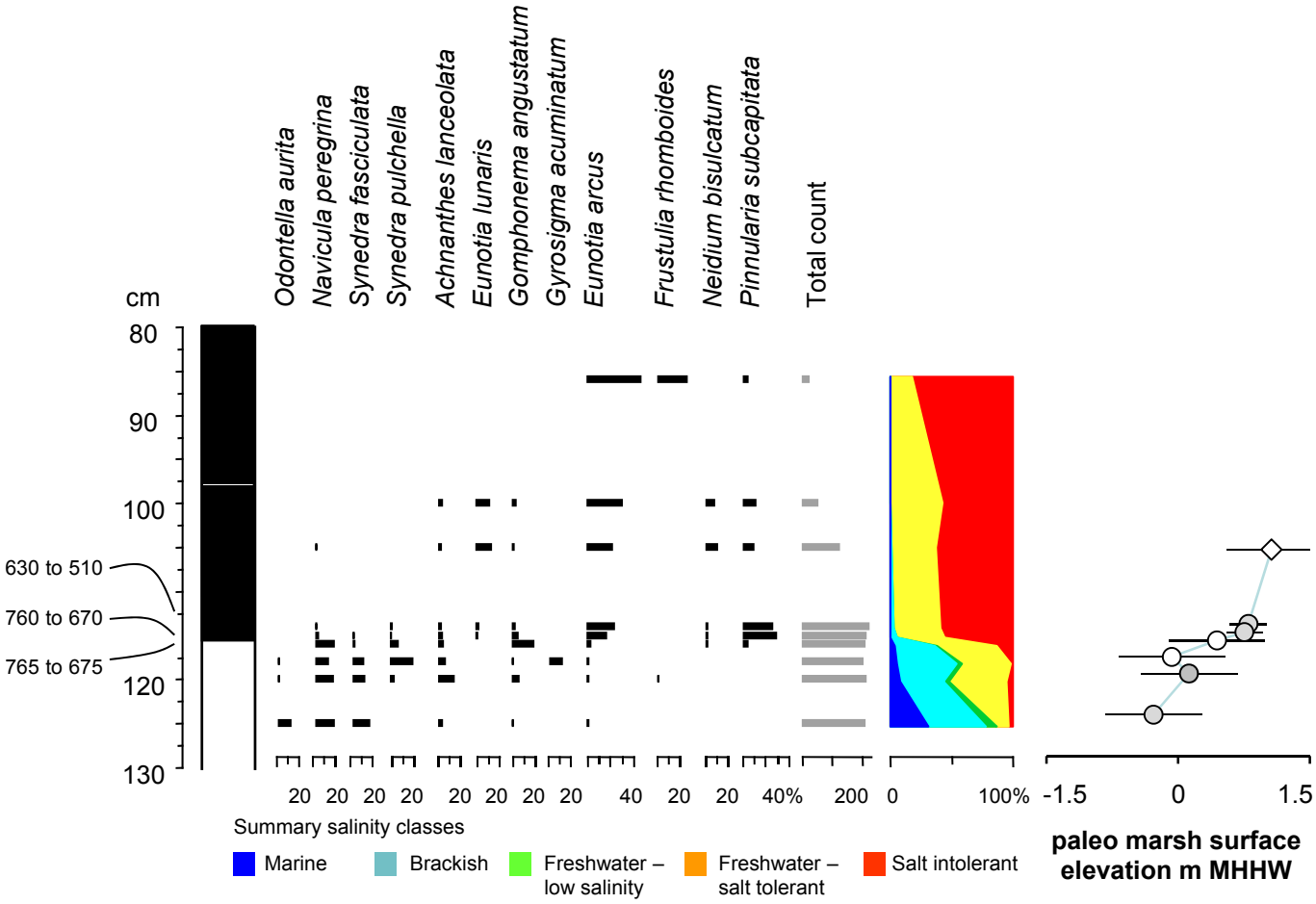
cm
80
90
100
120
130
630 to 510
760 to 670
765 to 675
Odontella aurita
Navicula peregrina
Synedra fasciculata
Synedra pulchella
Achnanthes lanceolata
Eunotia lunaris
Gomphonema angustatum
Gyrosigma acuminatum
Eunotia arcus
Frustulia rhomboides
Neidium bisulcatum
Pinnularia subcapitata
Total count
20 20 20 20 20 20 20 20 40 20 20 40% 200
0 100%
-1.5 0 1.5
paleo marsh surface elevation m MHHW
Summary salinity classes
Marine
Brackish
Freshwater – low salinity
Freshwater – salt tolerant
Salt intolerant

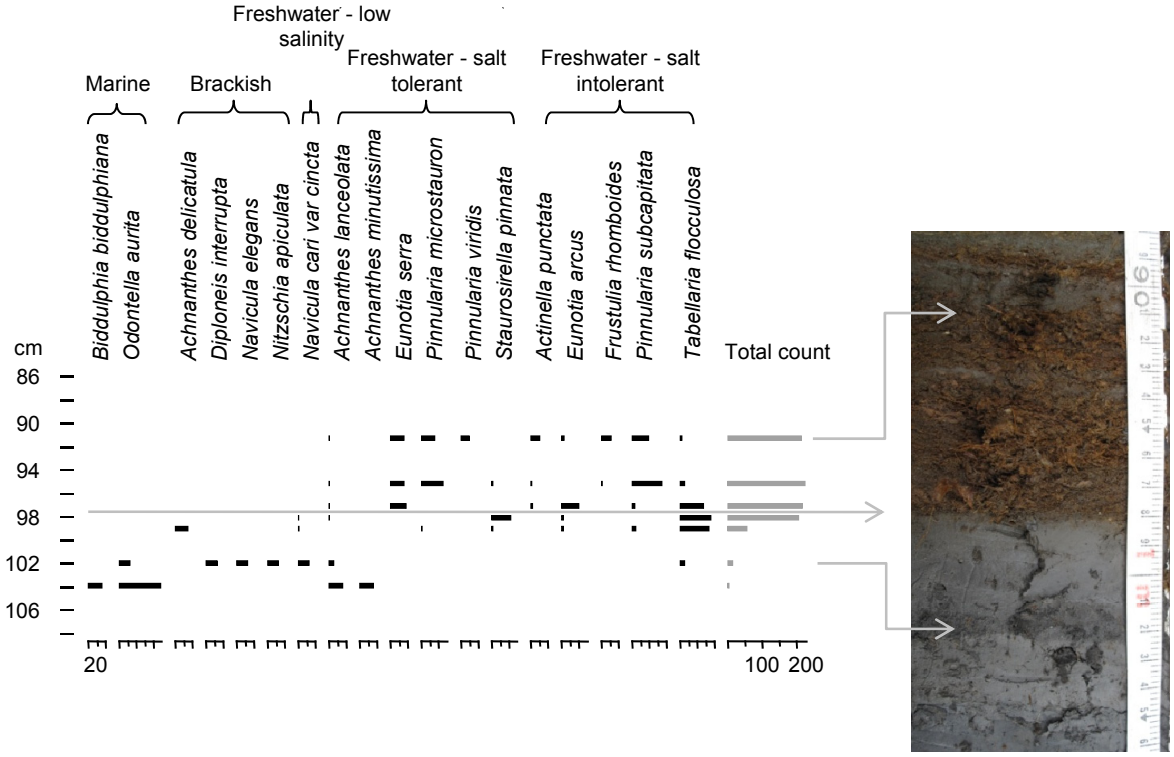
Freshwater - low salinity
Marine
Brackish
Freshwater - salt tolerant
Freshwater - salt intolerant
Biddulphia biddulphiana
Odontella aurita
Achnanthes delicatula
Diploneis interrupta
Navicula elegans
Nitzschia apiculata
Navicula cari var cincta
Achnanthes lanceolata
Achnanthes minutissima
Eunotia serra
Pinnularia microstauron
Pinnularia viridis
Staurosirella pinnata
Actinella punctata
Eunotia arcus
Frustulia rhomboides
Pinnularia subcapitata
Tabellaria flocculosa
Total count
cm
86
90
94
98
102
106
20
100
200


a


b


c

Radiocarbon age comparisons

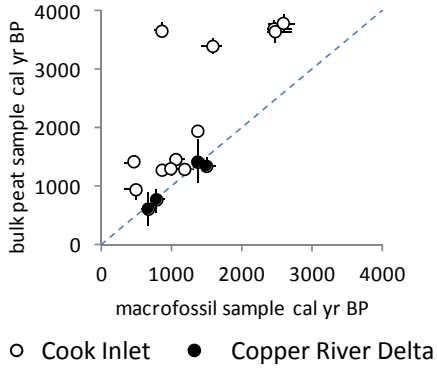

a) Full model structure

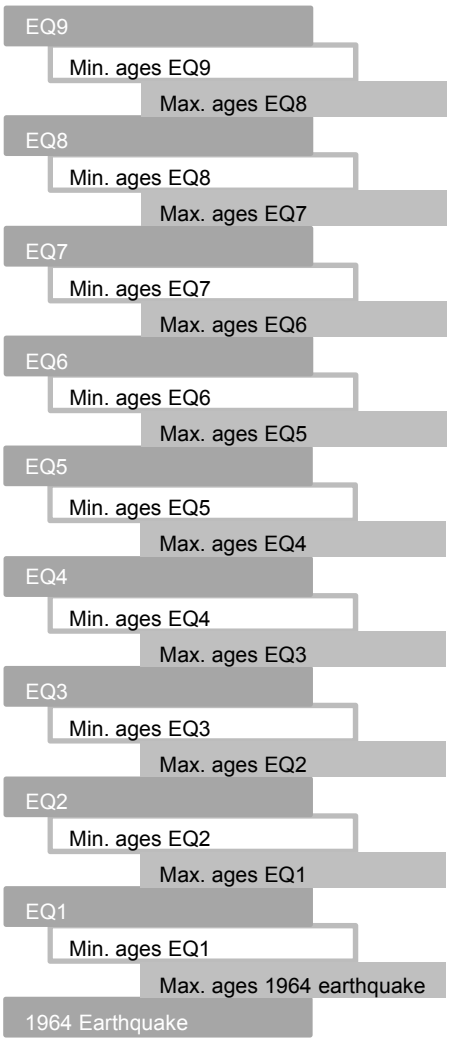

b) Example model output: EQ1

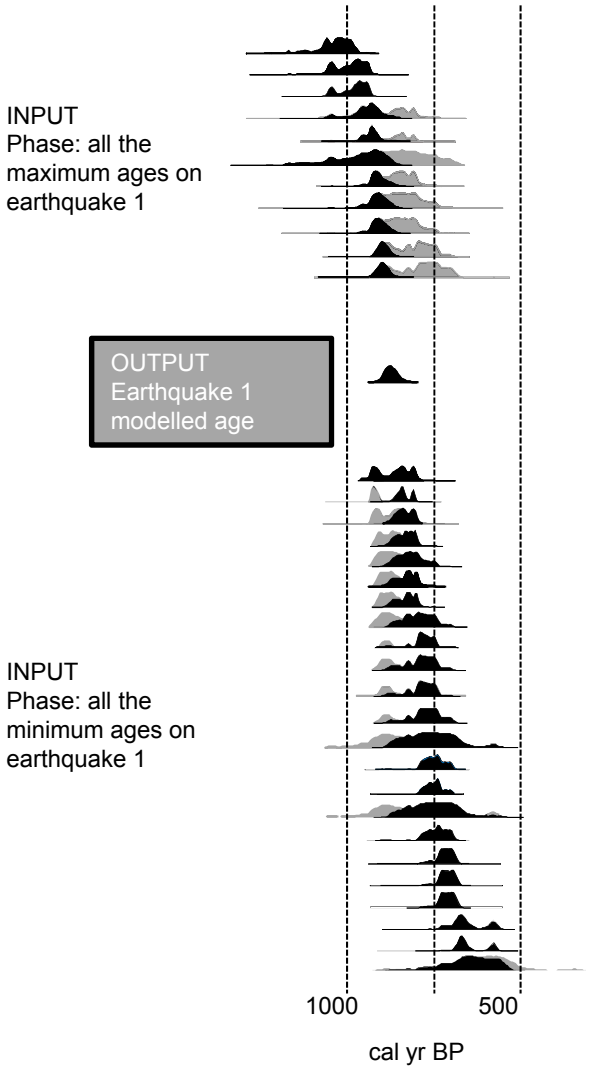

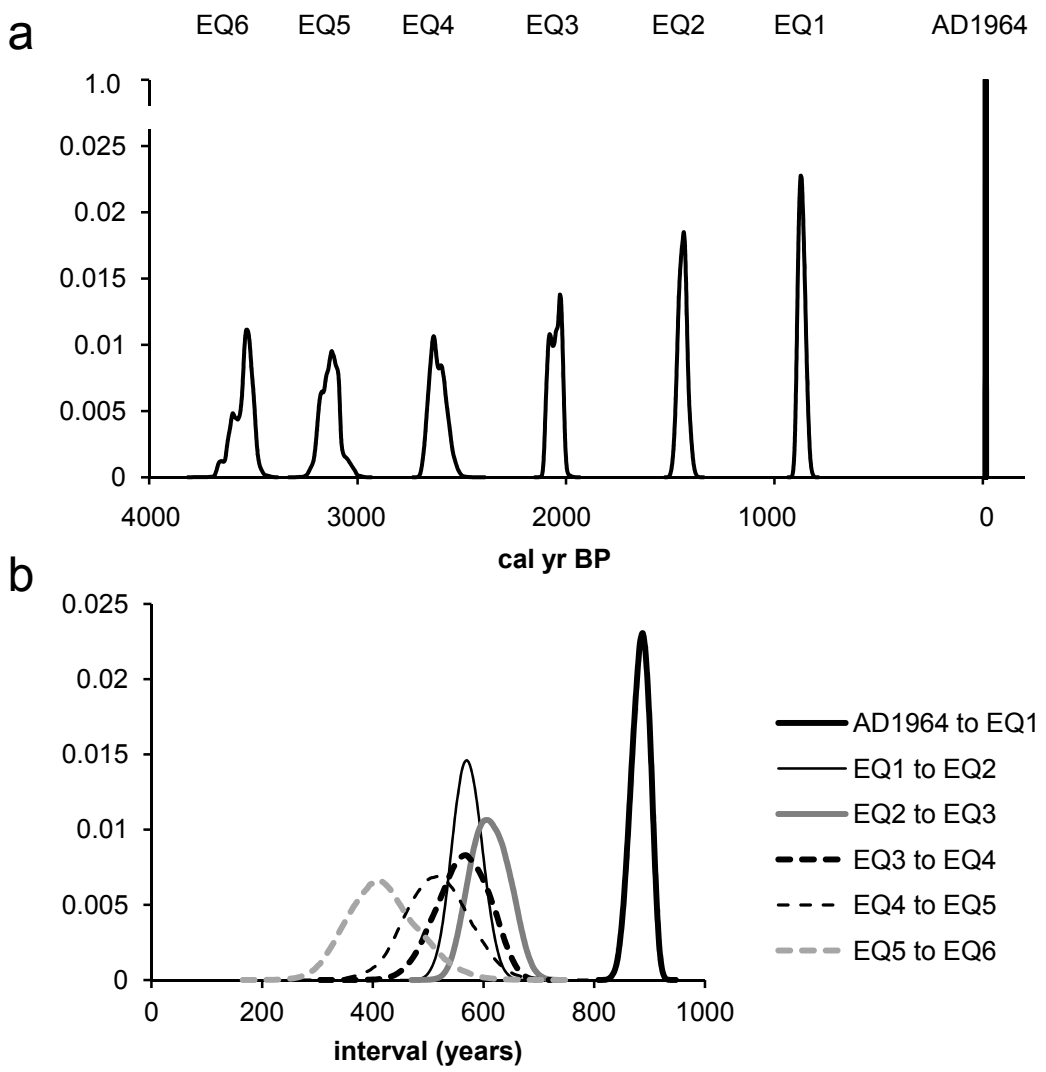
a
EQ6
EQ5
EQ4
EQ3
EQ2
EQ1
AD1964
1.0
0.025
0.02
0.015
0.01
0.005
0
4000
3000
2000
1000
0
cal yr BP
b
0.025
0.02
0.015
0.01
0.005
0
0
200
400
600
800
1000
interval (years)
AD1964 to EQ1
EQ1 to EQ2
EQ2 to EQ3
EQ3 to EQ4
EQ4 to EQ5
EQ5 to EQ6

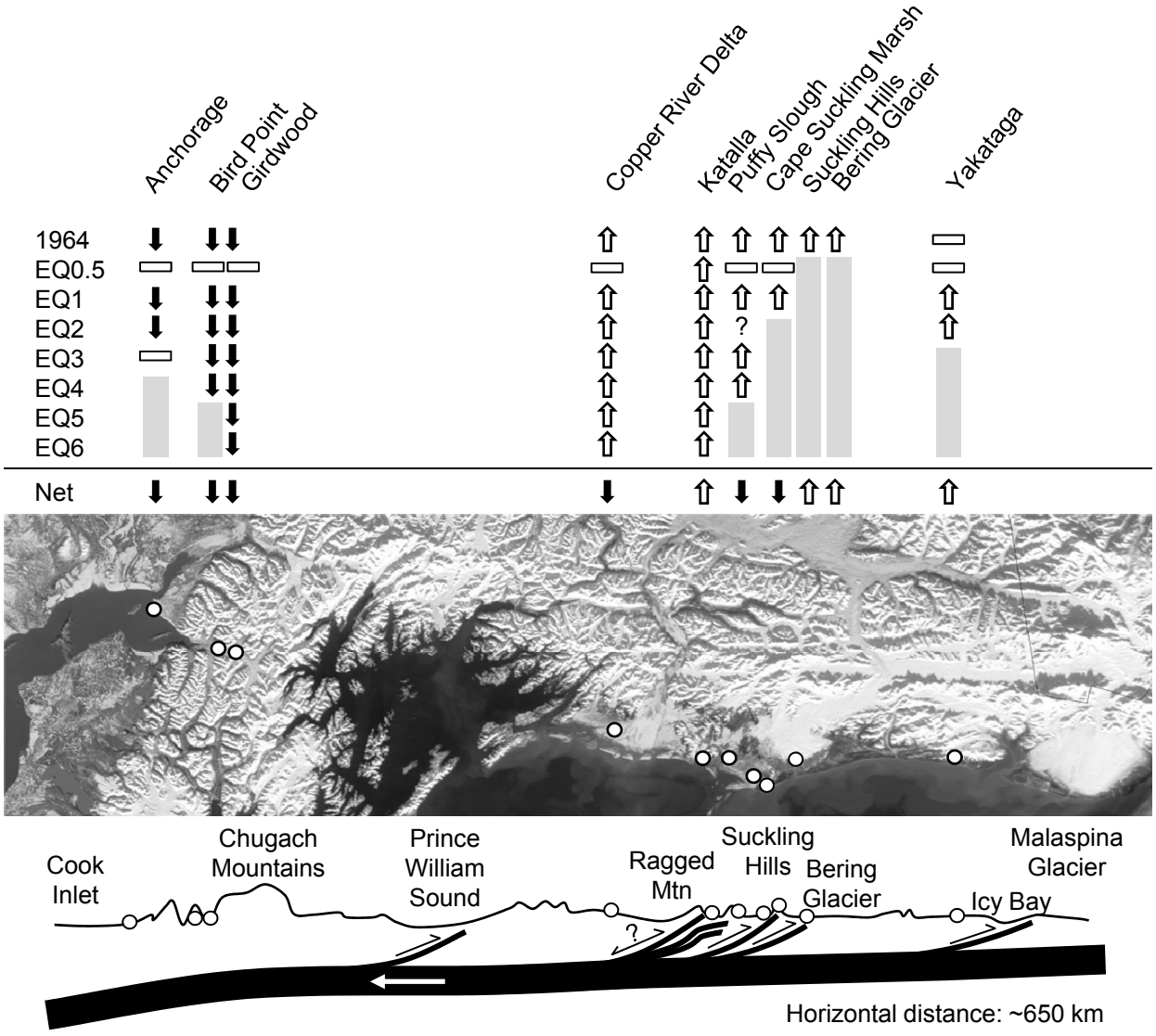
Anchorage
Bird Point
Girdwood
Copper River Delta
Katalla
Puffy Slough
Cape Suckling
Marsh
Suckling Hills
Bering Glacier
Yakataga
1964
EQ0.5
EQ1
EQ2
EQ3
EQ4
EQ5
EQ6
?
Net
Cook Inlet
Chugach Mountains
Prince William Sound
Ragged Mtn
Suckling Hills
Bering Glacier
Malaspina Glacier
Icy Bay
?
Horizontal distance: ~650 km

Table 1: Summary statistics for transfer function models used to reconstruct paleo marsh surface elevations. All models use modern samples from the regional-scale dataset covering sites across south-central Alaska (Full details of modern samples and model development in Hamilton and Shennan (2005) and Watcham et al., (2013)).

	Model 1	Model 2	Model 3
Number of samples in modern training set	100	206	255
Number of components in weighted averaging partial least squares model[1]	2	2	2
Squared correlation between bootstrap predicted and observed values (r^2)	0.75	0.68	0.76
Root mean squared error of prediction (bootstrap RMSEP)	6.31	11.94	17.48
Improvement in RMSEP over one-component model	14.7%	11.4%	10.5%
RMSEP scaled to tidal range at Katalla and Copper River Delta	0.10 m	0.19 m	0.27 m
Model applicable to lithology of fossil sample	Peat	Silt with herbaceous rootlets[2]	Silt , no visible rootlets

[1] We assessed model performance using r^2, scatterplots of observed and predicted values, and RMSEP, with the best models being those with the highest r^2 value, a linear distribution of observed plotted against predicted values, and the lowest RMSEP, but only if the RMSEP was improved by at least 5% with the addition of an extra component.

[2] Where there was no good or close modern analogue using model 2 for a silt unit with herbaceous rootlets we would apply model 3 if it gave at least a close modern analogue, indicating a better fit but with a larger uncertainty term.

Table 2: New Radiocarbon dates
All samples on herbaceous macrofossil stem/leaves picked from peat or silt matrix

Lab code	Site	Sample	Description	depth below core or section datum	core or section datum m MHHW	14C BP	SD	Range (cal yr BP)		
Copper River Delta: Alaganik Slough										
Beta-223760	AS 1	AS/06/1/2	Base of peat 1	110	~1	700	40	559	to	721
Beta-223761	AS 1	AS/06/1/3	Base of peat 2	310	~1	1610	40	1403	to	1601
Beta-266415	AS 3	AS/09/3/1	Base of peat 1	75	~1	880	20	733	to	901
Beta-266416	AS 3	AS/09/3/2	Base of peat 2	145	~1	1480	20	1318	to	1402
Beta-266417	AS 2	AS/09/4	Base of peat 1	75	~1	930	20	793	to	915
Beta-266418	AS 3	AS/09/5	Base of peat 3	436	~1	2020	20	1900	to	2037
Beta-266419	AS 2	AS/09/8	Base of peat 2	175	~1	1430	20	1296	to	1356
Katalla										
Beta - 318153	Ka 2.1	KR/07/1B/40	5cm above base of peat	40	~2.4	240	30	-1	to	424
Beta - 318154	Ka 2.1	KR/07/1B/42	3cm above base of peat	42	~2.4	270	30	0	to	435
Beta - 239237	Ka 2.1	KA/07/1A/45	Base of peat layer	45	~2.4	400	40	318	to	518
Beta - 239238	Ka 2.4	KA/07/4/71	Base of peat layer	71	~2.4	530	40	506	to	638
Beta - 316245	Ka 3.1	KR11-1-381	Within silt layer, above sand	381	~3.9	1510	30	1319	to	1515
Beta - 316246	Ka 5.3	KR11-3-35	Top of peat layer	35	~2	1740	30	1562	to	1715
Beta - 316247	Ka 5.3	KR11-3-50	1cm above base of peat layer	50	~2	2030	30	1898	to	2105
Beta - 316248	Ka 5.3	KR11-3-51	Base of peat layer	51	~2	2060	30	1948	to	2118
Beta - 316249	Ka 5.3	KR11-3-62	Top of peat layer	62	~2	2270	30	2158	to	2347
Beta - 316250	Ka 5.3	KR11-3-81	Base of peat layer	81	~2	2390	30	2344	to	2675
Beta - 316251	Ka 5.5	KR11-5-27	Base of peat layer above freshwater silt unit	27	~4.2	110	30	-4	to	269
Beta - 316252	Ka 5.5	KR11-5-96	1cm above base of peat layer	96	~4.2	830	30	686	to	789
Beta - 316253	Ka 5.5	KR11-5-97	Base of peat layer	97	~4.2	950	30	794	to	926
Beta - 316254	Ka 4.6	KR11-6-122	2cm above base of peat layer	122	~3.9	880	30	729	to	907
Beta - 316255	Ka 4.6	KR11-6-124	Base of peat layer	124	~3.9	840	30	685	to	892
Beta - 316256	Ka 4.6	KR11-6-127	Within silt layer, below peat contact	127	~3.9	1130	30	962	to	1167
Beta - 316257	Ka 4.8	KR11-8-190	Within silt layer, above sand	190	~3.9	1250	30	1082	to	1273
Beta - 316258	Ka 3.10	KR11-10-111	4cm above base of peat layer	111	~3.9	530	30	510	to	629
Beta - 316259	Ka 3.10	KR11-10-113	2cm above base of peat layer	113	~3.9	790	30	671	to	761
Beta - 316260	Ka 3.10	KR11-10-115	Base of peat layer	115	~3.9	800	30	675	to	765
Puffy Slough										
Beta - 328272	PF 4	PF/07/4 - 374	Base of lowest peat	374	~2	2370	40	2331	to	2682
Beta - 328271	PF 4	PF/07/4 - 370	Above base of lowest peat	370	~2	2170	30	2065	to	2311
Beta - 328270	PF 4	PF/07/4 - 260	Base of middle peat	260	~2	2120	30	1999	to	2293
Beta - 328269	PF 4	PF/07/4 - 258	2 cm above base of middle peat	258	~2	1320	30	1179	to	1298
Beta - 328268	PF 4	PF/07/4 - 153	Base of upper peat	153	~2	790	30	671	to	761
Beta - 328267	PF 4	PF/07/4 - 152	1cm above base of upper peat	152	~2	390	30	320	to	509

Table 3: Age model summary of earthquake ages and intervals. Oxcal model outputs for individual probability density functions, showing range (95.4% probability), mean, standard deviation, and median; and number of sites and number of samples recording each earthquake in model input. Older earthquakes not shown as they are less well constrained due to small sample sizes and are recorded at a single site.

Modelled age (years BP)	**from**	**to**	**%**	**μ**	**σ**	**m**	**n_{sites}**	**$n_{samples}$**
EQ1	902	837	95.4	870	17	871	9	34
EQ2	1484	1397	95.4	1440	21	1441	7	17
EQ3	2102	2006	95.4	2052	27	2050	6	9
EQ4	2685	2540	95.4	2615	38	2618	5	13
EQ5	3216	3037	95.4	3131	43	3131	2	5
EQ6	3662	3475	95.4	3550	47	3541	1	7
Modelled interval (years)								
AD1964 to EQ1	850	915	95.4	883	17	885		
EQ1 to EQ2	517	625	95.4	571	27	571		
EQ2 to EQ3	545	680	95.4	611	35	611		
EQ3 to EQ4	470	653	95.4	563	47	565		
EQ4 to EQ5	403	635	95.4	517	58	516		
EQ5 to EQ6	299	550	95.4	419	64	415		
Mean interval AD1964 to EQ6	518	558	95.4	536	10	535		
Mean interval EQ1 to EQ6	579	612	95.4	594	8	593		

Shennan et al: supplementray information table
Radioacrbon data and age model structure for Oxcal age modelling

Site Codes
Kas Kasilof; Ke Kenai; Anc Anchorage; BP Bird Point; Gw Girdwood; CRD Copper River Delta; Kat Katalla; PS Puffy Slough; CS Cape Suckling; Ya Yakataga Coast

Literature sources
New: this paper table 2
1: Carver & Plafker 2008
2: Shennan et al. 2008
3: Barlow et al., 2012
4: Hamilton & Shennan, 2005
5: Shennan & Hamilton, 2006
6: Hamilton et al., 2005
7: Shennan 2009
8: Shennan et al., 2009

Lab code	14C BP	SD	Site	Sample code	Source	Description	Boundary	Constraint
							Earthquake 9	
W-6356	4860	90	CRD	91APR604N2	1	Alaganic Slough 0.5km below boat ramp		Minimum
W6360	4650	100	CRD	91APR606Y	1	Upper Alaganic Slough redrill		Minimum
							Earthquake 8	
CAMS-16583	4340	90	CRD	93APR25R	1	Alaganic Slough 0.1km above boat ramp		Minimum
CAMS-16573	4210	60	CRD	93APR21SS	1	Alaganic Slough 0.5km below boat ramp		Minimum
W-6355	4180	80	CRD	91APR604L	1	Alaganic Slough 0.5km below boat ramp		Minimum
CAMS-16579	3810	70	CRD	93APR23W	1	Alaganic Slough 1.4km above boat ramp		Minimum
							Earthquake 7	
W-6353	3690	50	CRD	91APR604I	1	Alaganic Slough 0.5km below boat ramp		Minimum
CAMS-16581	3680	60	CRD	93APR25N	1	Alaganic Slough 0.1km above boat ramp		Minimum
CAMS-16578	3640	90	CRD	93APR23T	1	Alaganic Slough 1.4km above boat ramp		Minimum
W6358	3600	90	CRD	91APR606R	1	Upper Alaganic Slough redrill		Minimum
							Phase boundary	
Beta-223764	3490	40	Gw	GW5/1	2	Upper boundary of Girdwood peat Y		Maximum
CAMS-16577	3280	60	CRD	93APR23M	1	Alaganic Slough 1.4km above boat ramp		Maximum

AA5640	3202	57	CRD	89APR502X	1	100 m upstream of boat ramp	Maximum
						Earthquake 6	
W6549	3420	60	CRD	93APR25G	1	Alaganic Slough 0.1km above boat ramp	Minimum
AA5764	3279	102	CRD	89APR503M	1	Upper Alaganic Slough	Minimum
CAMS-16572	3180	60	CRD	93APR21FF	1	Alaganic Slough 0.5km below boat ramp	Minimum
AA5639?	3096	73	CRD	89APR502W	1	100 m upstream of boat ramp	Minimum
CAMS-16576	3060	60	CRD	93APR23L	1	Alaganic Slough 1.4km above boat ramp	Minimum
						Phase boundary	
Beta-184329	3040	40	Gw	G/03/4P#20	2	Upper boundary of Girdwood peat A	Maximum
Beta-223766	3020	40	Gw	GW5/3	2	Upper boundary of Girdwood peat A	Maximum
Beta-223763	3010	40	Gw	GW1/1	2	Upper boundary of Girdwood peat A	Maximum
Beta-223767	2930	40	Gw	GW6/1	2	Upper boundary of Girdwood peat A	Maximum
						Earthquake 5	
W6547	3070	50	CRD	93APR21AA	1	Alaganic Slough 0.5km below boat ramp	Minimum
						Phase boundary	
AA4905	2855	95	CRD	89APR503J	1	Upper Alaganic Slough	Maximum
AA5637	2662	67	CRD	89APR502O	1	100 m upstream of boat ramp	Maximum
Beta-266422	2580	20	BP	BP/09/1/3	3	Top of Bird Point peat D	Maximum
Beta-184327	2560	40	Gw	G/03/4P#18	2	Top of Girdwood peat D	Maximum
Beta-223768	2490	40	Gw	GW6/2	2	Top of Girdwood peat D	Maximum
CAMS-93961	2425	35	Gw	GW/02/1C#5	2	Top of Girdwood peat D	Maximum
						Earthquake 4	
AA5644	2614	89	CRD	89APR503I	1	Upper Alaganic Slough	Minimum
AA5636	2614	65	CRD	89APR502M	1	100 m upstream of boat ramp	Minimum
CAMS-16574	2570	60	CRD	93APR21W	1	Alaganic Slough 0.5km below boat ramp	Minimum
W6452	2550	90	CRD	91APR606H	1	Upper Alaganic Slough redrill	Minimum
Beta - 316250	2390	30	Kat	KR11-3-81	new	Base of peat layer	Minimum
Beta - 328272	2370	40	PS	PF/07/4 - 374	new	Puffy Slough 4 - base of lowest peat	Minimum
AA4892	2342	78	CRD	89APR503G	1	Upper Alaganic Slough	Minimum
						Phase boundary	
Beta-266421	2170	20	BP	BP/09/1/2	2	Top of Bird Point peat E	Maximum
AA-48170	2140	47	Gw	GW1A-20	2	Top of Girdwood peat E	Maximum
Beta-184324	2120	50	Gw	G/03/3#15	2	Top of Girdwood peat E	Maximum
Beta-266423	2040	20	Hope	HP/09/8	3	Top of Hope fourth peat (E)	Maximum
						Earthquake 3	

Beta - 328270	2120	30	PS	PF/07/4 - 260	new	Puffy Slough 4 - base of middle peat	Minimum
Beta - 316248	2060	30	Kat	KR11-3-51	new	Base of peat layer	Minimum
Beta - 316247	2030	30	Kat	KR11-3-50	new	1cm above base of peat layer	Minimum
Beta-266418	2020	20	CRD	AS/09/5	1	Bottom of Alaganic Slough peat 3	Minimum
AA4890	1882	72	CRD	89APR503F	1	Upper Alaganic Slough	Minimum
							Phase boundary
Beta-184332	1670	40	Ke	KE/03/5#23	4	Top of Kenai peat A	Maximum
CAMS-93964	1670	45	Ke	KE/2000/7#8	4	Top of Kenai peat A	Maximum
W6085	1610	220	CRD	88APR11B	1	Pete Dahl Cutoff	Maximum
Beta-266420	1580	20	BP	BP/09/1/1	3	Top of Bird Point peat F	Maximum
CAMS-93966	1570	35	Kas	KS/01/1#10	5	Top of Kasilof lowest peat	Maximum
Beta-184326	1540	40	Gw	G/03/2#17	2	Top of Girdwood peat F	Maximum
Beta-184318	1530	40	Anc	OV/02/2#9	6	Top of Ocean View peat C	Maximum
Beta-184311	1500	40	Anc	OV/03/23#2	6	Top of Ocean View peat C	Maximum
							Earthquake 2
Beta-223761	1610	40	CRD	AS1/3	new	Bottom boundary of peat 'A'	Minimum
W6361	1540	60	CRD	91APR609J	1	Upper Alaganic Slough	Minimum
Beta - 316245	1510	30	Kat	KR11-1-381	new	Stems within silt layer, above sand	Minimum
W6088	1500	160	CRD	88APR11 C	1	Pete Dahl Cutoff	Minimum
Beta-266416	1480	20	CRD	AS/09/3/2	1	Bottom of Alaganic Slough peat 2	Minimum
W6454	1480	80	CRD	91APR606C	1	Upper Alaganic Slough redrill	Minimum
AA4897	1451	49	CRD	89APR503D	1	Upper Alaganic Slough	Minimum
AA4893	1446	56	CRD	89APR502F	1	100 m upstream of boat ramp	Minimum
Beta-266419	1430	20	CRD	AS/09/8	new	Bottom of Alaganic Slough peat 2	Minimum
							Phase boundary
Beta - 316256	1130	30	Kat	KR11-6-127	new	Within silt layer, below peat contact	Maximum
Beta-184315	1070	40	Anc	OV/01/1B#6	6	Top of Ocean View peat D	Maximum
SUERC-22676	1060	37	BP	BP086R12	3	Top of Bird Point peat G	Maximum
AA5624	998	56	CRD	88APR13AA	new	Lower Pete Dahl Slough	Maximum
SUERC-22673	991	35	BP	BP086R11	3	Top of Bird Point peat G	Maximum
W6098	960	120	CRD	88APR11H	1	Pete Dahl Cutoff	Maximum
CAMS-93958	955	40	Gw	GW/02/1B#2	2	Top of Girdwood peat G	Maximum
Beta-45199	940	60	Gw	GW91-4-1	2	Rooted wood at top of Girdwood peat G	Maximum
Beta-184317	940	50	Anc	OV/03/25#8	6	Top of Ocean View peat D	Maximum
Beta-184321	890	40	Gw	G/03/1#12	2	Top of Girdwood peat G	Maximum

Beta-45197	860	60	Gw	GW91-2-1	2	Rooted wood at top of Girdwood peat G	Maximum
						Earthquake 1	
Beta - 212211	970	40	CS	CS 05/2 268cm	7	herbaceous roots/stems, base of peat	Minimum
Beta-242795	970	20	Ya	YK/5-2	8	herbaceous roots/stems, base of peat	Minimum
Beta - 316253	950	30	Kat	KR11-5-97	new	herbaceous roots/stems, base of peat	Minimum
Beta-266417	930	20	CRD	AS/09/4	new	Bottom of Alaganic Slough peat 1	Minimum
Beta - 212213	920	40	CS	CS 05 2 269cm	7	Plant fragment in 1 cm sand below peat layer	Minimum
Beta-239243	920	20	Ya	YK/2	8	herbaceous roots/stems, base of peat	Minimum
Beta-239245	920	20	Ya	YK/5-1	8	herbaceous roots/stems, 3 cm above base of peat	Minimum
M2873	895	50	CRD	89APR505H rer	1	Tiedemann Slough	Minimum
Beta-266415	880	20	CRD	AS/09/3/1	new	Bottom of Alaganic Slough peat 1	Minimum
Beta - 212212	880	40	CS	CS 05/2 266cm	7	herbaceous roots/stems, 2cm above base of peat	Minimum
Beta - 316254	880	30	Kat	KR11-6-122	new	2cm above base of peat layer	Minimum
M2874	865	45	CRD	89APR505H	1	Tiedemann Slough	Minimum
W6123	850	120	CRD	88APR13B	1	Lower Pete Dahl Slough	Minimum
Beta - 316255	840	30	Kat	KR11-6-124	new	herbaceous roots/stems, base of peat	Minimum
Beta-239239	840	20	PS	Puffy_Slough	new	herbaceous roots/stems, base of peat	Minimum
W6102	830	120	CRD	88APR11I	1	Pete Dahl Cutoff	Minimum
Beta - 316252	830	30	Kat	KR11-5-96	new	1cm above base of peat layer	Minimum
Beta - 316260	800	30	Kat	KR11-10-115	new	herbaceous roots/stems, base of peat	Minimum
Beta - 316259	790	30	Kat	KR11-10-113	new	2cm above base of peat layer	Minimum
Beta - 328268	790	30	PS	PF/07/4 - 153	new	Puffy Slough 4 - base of upper peat	Minimum
AA5626	706	54	CRD	88APR16A	1	Alaganic Slough boat ramp	Minimum
Beta-223760	700	40	CRD	AS1/2	new	Bottom boundary of peat 'B'	Minimum
W6139	630	140	CRD	88APR16C	1	Alaganic Slough boat ramp	Minimum
						Earthquake 0.5	
Beta - 239238	530	40	Kat	KA/07/4/71	new	herbaceous roots/stems, base of peat	Minimum
Beta - 239237	400	40	Kat	KA/07A/1/45	new	herbaceous roots/stems, base of peat	Minimum
Beta - 318154	270	30	Kat	KR-07B-1-42	new	Herbaceous leaf/stem fragments	Minimum